

AD-A093 131

MASSACHUSETTS INST OF TECH CAMBRIDGE DEPT OF MATERIA--ETC F/6 11/6
XPS/AES STUDIES OF ALUMINUM FRACTURE SURFACES.(U)

NOV 80 B L AVERBACH

AFOSR-76-2924

UNCLASSIFIED

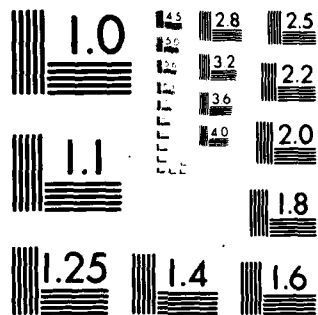
AFOSR-TR-80-1216

NL

Fig 1
Al 2p
2846.5



END
DATE
FILMED
1-81
DTIC



MICROCOPY RESOLUTION TEST CHART

NATIONAL BUREAU OF STANDARDS-1963-A

41
AFOSR-TR-80-1216

LEVEL

12

XPS/AES Studies of Aluminum Fracture Surfaces

by

B. L. Averbach

Department of Materials Science
Massachusetts Institute of Technology
Cambridge, Massachusetts 02139

Final Technical Report

November 15, 1980

Air Force Office of Scientific Research
Contract Number AFOSR-76-2924

40940 500
Approved for public release;
distribution unlimited.

80 12 22 140

AD A093131

DDC FILE COPY

Unclassified

SECURITY CLASSIFICATION OF THIS PAGE (When Data Entered)

(19) REPORT DOCUMENTATION PAGE		READ INSTRUCTIONS BEFORE COMPLETING FORM
1. REPORT NUMBER (18) AFOSR TR-80-1216	2. GOVT ACCESSION NO. AD-A093131	3. RECIPIENT'S CATALOG NUMBER
4. TITLE (and Subtitle) (6) XPS/AES STUDIES OF ALUMINUM FRACTURE SURFACES		5. TYPE OF REPORT & PERIOD COVERED (9) FINAL rept.
7. AUTHOR(s) (10) B. L. AVERBACH		6. PERFORMING ORG. REPORT NUMBER
9. PERFORMING ORGANIZATION NAME AND ADDRESS Massachusetts Institute of Technology Cambridge, Massachusetts 02139		8. CONTRACT OR GRANT NUMBER(s) (15) AFOSR-76-2924
11. CONTROLLING OFFICE NAME AND ADDRESS Air Force Office of Scientific Research Building 410 Bolling Air Force Base, D.C. 20332 <i>NE</i>		10. PROGRAM ELEMENT, PROJECT, TASK AREA & WORK UNIT NUMBERS (16) 2306A2 - 61102F 11A2
14. MONITORING AGENCY NAME & ADDRESS (if different from Controlling Office)		12. REPORT DATE (11) 15 November 15, 1980
		13. NUMBER OF PAGES 52 (12) 531
		15. SECURITY CLASS. (of this report) Unclassified
		15a. DECLASSIFICATION/DOWNGRADING SCHEDULE
16. DISTRIBUTION STATEMENT (of this Report) <div style="border: 1px solid black; padding: 5px; text-align: center;"> DISTRIBUTION STATEMENT A Approved for public release; Distribution Unlimited </div>		
17. DISTRIBUTION STATEMENT (of the abstract entered in Block 20, if different from Report)		
18. SUPPLEMENTARY NOTES		
19. KEY WORDS (Continue on reverse side if necessary and identify by block number)		
Aluminum Surface Fracture	XPS ESCA AES	SAM Chemical Shift
20. ABSTRACT (Continue on reverse side if necessary and identify by block number)		
<p>X-ray photoemission (XPS, or ESCA) and Auger electron scattering (AES) studies were made of aluminum alloy surfaces after polishing, etching and ion bombardment, and in the as-received condition. Surfaces obtained on fracture at 10⁻¹⁰ torr were also studied by means of scanning Auger microscopy (SAM). The materials studied were 2024-T351,</p> <p style="text-align: right;">409463 JOB</p>		

Unclassified

SECURITY CLASSIFICATION OF THIS PAGE (When Data Entered)

7075-T651 and high purity aluminum. Aluminum was found to exist in two chemical states at the surfaces of these materials. The Al 2p line of the XPS spectra was observed at 75.8 ± 0.2 eV corresponding to the oxide phase, for the as-received and the polished surfaces, and at 72.6 ± 0.2 eV, corresponding to metallic aluminum, for surfaces cleaned by prolonged argon-ion bombardment. Specimens which had been etched or partially cleaned by ion bombardment exhibited both peaks, separated by the chemical shift of 3.2 eV. A similar chemical shift, previously unreported, was observed for the Al 2s line, with the aluminum oxide line at 120.5 ± 0.5 eV and the metallic line at 118.0 ± 0.2 eV, with a chemical shift of 2.5 eV. Contaminants could not be eliminated entirely, even after prolonged ion-bombardment. XPS oxygen, O 1s, lines at 531.0 ± 0.4 eV, corresponding to alumina, were observed for all surfaces which had been etched or bombarded with argon-ions. Specimens in the polished or as-received condition exhibited O 1s peaks at 533.1 ± 0.2 eV, characteristic of the hydroxide phase or of a combination of the oxide and adsorbed water. Clean aluminum spectra were observed only at surfaces fractured in the SAM apparatus at 10^{-10} torr. Bulk plasmon loss peaks separated by 15.7 eV were observed near the 2 kV calibration elastic peak, confirming that the aluminum fracture surfaces were uncontaminated. Attempts were made, using SAM scans, to find grain boundary effects near the surfaces of aluminum alloys embrittled by exposure to water-vapor-saturated air at 70°C for 24 hours. There were slight shifts in the KLL Auger spectra at some grain boundary intersections with the surface, but the resolution was inadequate to allow definitive observations.

UNCLASSIFIED

TABLE OF CONTENTS

	<u>Page</u>
Abstract -----	1
Introduction -----	2
Experimental Results -----	6
Specimen Preparation -----	6
XPS/AES Analysis Parameters -----	7
XPS/AES Results -----	10
High Resolution XPS Spectra -----	12
Oxygen: High Resolution XPS Spectra -----	14
Aluminum Fracture Surfaces: SAM Spectra -----	15
Specimens in Water-Vapor-Saturated Sir -----	16
Summary and Conclusions -----	18
Acknowledgements -----	22
References -----	23
Figures -----	25

AIR FORCE OFFICE OF SCIENTIFIC RESEARCH (AFSC)
 NOTICE OF TRANSMITTAL TO DDC
 This technical report has been reviewed and is
 approved for public release IAW AFR 190-12 (7b).
 Distribution is unlimited.
 A. D. BLOSE
 Technical Information Officer

(AFSC)

is
 190-12 (7b)

Technical Information Officer

Accession For	
NTIS GRA&I	<input type="checkbox"/>
DTIC TAB	<input type="checkbox"/>
Unannounced	<input type="checkbox"/>
Justification	<input type="checkbox"/>
By _____	
Distribution/	
Availability Codes	
Dist	Avail and/or Special
A	

LIST OF FIGURES

<u>Figure</u>		<u>Page</u>
1	Gold: XPS Wide Scan Spectra -----	25
2	Gold: XPS High Resolution Spectra (Au 4f _{5/2} & Au 4f _{7/2} Regions) -----	26
3	Aluminum: XPS Wide Scan Spectra -----	27
4	Pure Aluminum: AES Wide Scan Spectrum -----	28
5	2024-T351 Aluminum: AES Wide Scan Spectra -----	29
6	7075-T651 Aluminum: AES Wide Scan Spectra -----	30
7	Aluminum: AES High Resolution Spectra -----	31
8	Pure Aluminum: XPS High Resolution Spectra (Aluminum Al 2p & Al 2s Regions) -----	32
9	2024-T351 Aluminum: XPS High Resolution Spectra (Aluminum Al 2p & Al 2s Regions) -----	33
10	7075-T651 Aluminum: XPS High Resolution Spectra (Aluminum Al 2p & Al 2s Regions) -----	34
11	Pure Aluminum: XPS High Resolution Spectra (Oxygen O 1s Region) -----	35
12	2024-T351 Aluminum: XPS High Resolution Spectra (Oxygen O 1s Region) -----	36
13	7075-T651 Aluminum: XPS High Resolution Spectra (Oxygen O 1s Region) -----	37
14	Gold & Aluminum: XPS High Resolution Spectra (Oxygen O 1s Region) -----	38
15	2024-T351 Aluminum Fracture Surface: SAM Wide Scan Spectrum -----	39
16	7075-T651 Aluminum Fracture Surface: SAM Wide Scan Spectrum -----	40
17	Aluminum Fracture Surfaces: SAM High Resolution Spectra -----	41

<u>Figure</u>		<u>Page</u>
18	2024-T351 Aluminum Fracture Surface: SAM High Resolution Spectrum -----	42
19	Pure Aluminum, exposed to water-vapor- saturated air at 70°C for 24 hours -----	43
20	2024-T351 Aluminum, exposed to water-vapor- saturated air at 70°C for 24 hours -----	44
21	7075-T351 Aluminum, exposed to water-vapor-saturated air at 70°C for 24 hours -----	45
22	SAM spectra from clean Al fracture surface and from surface exposed to water-vapor-saturated air at 70°C -----	46
23	SAM spectra from clean Al fracture surface and from surface exposed to water-vapor-saturated air at 70°C -----	47

XPS/AES Studies of Aluminum Fracture Surfaces

B. L. Averbach

Department of Materials Science and Engineering
 Massachusetts Institute of Technology
 Cambridge, Massachusetts 02139

ABSTRACT

X-ray photoemission (XPS, or ESCA) and Auger electron scattering (AES) studies were made of aluminum alloy surfaces after polishing, etching, and ion bombardment, and in the as-received condition. Surfaces obtained on fracture at ~~10⁻¹⁰~~ ^{10⁻¹⁰ to 10⁻¹¹ TH power} torr were also studied by means of scanning Auger microscopy (SAM). The materials studied were 2024-T351, 7075-T651 and high purity aluminum. Aluminum was found to exist in two chemical states at the surfaces of these materials. The Al 2p line of the XPS spectra was observed at 75.8 ± 0.2 eV, corresponding to the oxide phase, for the as-received and the polished surfaces, and at 72.6 ± 0.2 eV corresponding to metallic aluminum, for surfaces cleaned by prolonged argon-ion bombardment. Specimens which had been etched or partially cleaned by ion bombardment exhibited both peaks, separated by the chemical shift of 3.2 eV. A similar chemical shift, previously unreported, was observed for the Al 2s line, with the aluminum oxide line at 120.5 ± 0.5 eV and the metallic aluminum line at 110.0 ± 0.2 eV with a chemical shift of 2.5 eV. Contaminants could not be eliminated entirely, even after prolonged ion-bombardment. XPS oxygen, O 1s, lines at 531.0 ± 0.4 eV, corresponding to alumina, was observed for all surfaces which had been etched or bombarded with argon-ions. Specimens in the polished or as-received condition exhibited O 1s peaks at 533.1 ± 0.2 eV, characteristic of the hydroxide phase or of a combination of the oxide and adsorbed water. Clean aluminum spectra were observed only at surfaces fractured in the SAM apparatus at 10⁻¹⁰ torr. Bulk plasmon loss peaks separated by 15.7 eV were observed near the 2 kV calibration elastic peak, confirming that the aluminum fracture surfaces were uncontaminated. Attempts were made, using SAM scans, to find grain boundary effects near the surfaces of aluminum alloys embrittled by exposure to water-vapor-saturated air at 70°C for 24 hours. There were slight shifts in the KLL Auger spectra at some grain boundary intersections with the surface, but the resolution was inadequate to allow definitive observations.

10 to 10⁻¹¹
 TH power

+ or -

+ or -

+ or -

INTRODUCTION

Surfaces of aluminum alloys have been studied by a variety of methods such as gravimetric analysis (1, 2, 3, 4), and work function measurements (5, 6, 7, 8, 9, 10). More recently, secondary ion emission, SIMS, (11) and x-ray photoemission, i.e. XPS or ESCA, and Auger electron spectroscopy, AES, (12, 13) have been used to characterize the early stages of the chemisorption of oxygen on aluminum (11) and of early oxide growth (14). The preparation of atomically clean aluminum surfaces, however, presents special problems because of the reactivity of aluminum. It was shown by Jona (15) that (111), (100) and (110) surfaces of an aluminum single crystal which had been cleaned by argon-ion bombardment and annealing exhibited LEED patterns which were apparently those of clean aluminum surfaces. However, the effects of Argon-ion bombardment on several metal-oxide systems have been studied by XPS, and damage from ion beam bombardment has been detected (16, 17).

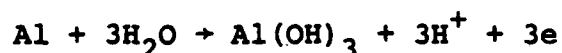
The various investigations into the initial stages of aluminum oxidation have not produced mechanisms of the surface reactions which are generally accepted (18, 19, 14). The effects of surface reactions on the mechanical properties, however, are well recognized. Leach (20) has reviewed much of the literature on the formation of surface films on aluminum alloys. He noted that the nature of the

surface layer is dependent on the oxidation rate. Oxide films grown on pure aluminum under near equilibrium conditions tend to be crystalline. At atmospheric temperature and pressure, however, the initial layers of oxide are formed on aluminum very rapidly and under non-equilibrium conditions, and the resistant surface structures appear to be amorphous. Leach also has noted that the oxide films apparently have mechanical properties which differ from those of the bulk oxide, and that the properties of metals are modified by the surface oxide films.

Grosskreutz (21) has examined the fatigue behavior of aluminum both in air and in vacuum. He found that the number of cycles required to initiate a microcrack increased as the ambient pressure was reduced. This was interpreted in terms of the effects of surface films on sources of dislocations at the surface. This was in agreement with Garrett and Knott (22) who showed that the presence of water vapor increased the fatigue crack growth rate in both commercial (2024-T6) and in pure aluminum-copper alloys (Al-3 Cu). The effect of water vapor on stress corrosion cracking and on embrittlement in commercial (7075) and high purity aluminum alloys (Al-6 Zn-3 Mg) has been studied by Scamans and Tuck (23) and by Scamans, Alani and Swann (24). It was postulated that intergranular hydrogen penetration was the

cause of the embrittlement produced by the water vapor. Diffusion of hydrogen along the grain boundaries was ascribed to the rapid formation of hydrogen at grain boundary-surface intersections, where rapid breakdown of the protective film occurred by a mechanism of hydrogen-induced blistering. Embrittlement of a stress corrosion cracking type was observed in an Al-6 Zn-3 Mg alloy with the degree of embrittlement increasing with time and temperature of exposure. However, the ductility of pre-exposed specimens could be restored by tensile testing in a vacuum. The rate of embrittlement was reduced by adding 1.7% copper or 0.14% chromium to the alloy, and the embrittlement rate in commercial 7075 alloy was also found to be smaller than that of the high purity alloy. Presumably, the chromium and copper phases acted as hydrogen traps.

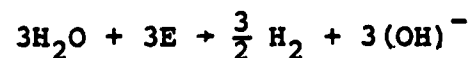
The reaction of aluminum with water vapor (23) at temperatures in the vicinity of 70°C produces a duplex film consisting of pseudoboehmite, which is an aluminum oxyhydroxide similar to boehmite (AlOOH) but containing more water, and boeyerite Al(OH)₃. The reactions may be written:



and



and



Hydrogen is produced in either the $\text{Al}(\text{OH})_3$ or the AlOOH reactions. However, the reaction of aluminum with water-vapor-saturated air as opposed to liquid water has received little attention. Information is particularly limited with respect to the effects of alloying elements. On the whole, it appears that the reduction in physical properties may be caused by an intergranular diffusion of hydrogen, but evidence for this is indirect and based largely on kinetic arguments. These arguments are based on the premise that only hydrogen can diffuse rapidly enough to produce the embrittlement at the observed rate.

In this study we have attempted to study the surface compounds which are produced in air and water vapor on two alloys, 2024 and 7075, as well as on pure aluminum. XPS (ESCA) observations of both Al and O peaks were used in an effort to identify the first stages of oxide formation. We found it difficult indeed to produce starting surfaces of suitable cleanliness and eventually found that only surfaces produced by fracture in the XPS equipment at 10^{-10} torr were clean. We also fractured specimens pre-exposed to water-vapor-saturated air and observed qualitatively that these specimens had been embrittled. We were unable, however, to observe any evidence of oxygen penetration at grain boundaries near the surface. We had postulated that the easy initiation of fatigue cracks was associated with oxide penetration at grain

boundary/surface intersections. The resolution was inadequate to detect the oxide penetration at grain boundaries, but the mechanism has not been ruled out.

EXPERIMENTAL RESULTS

Specimen Preparation

Specimens of 2024-T351 and 7075-T651 aluminum alloys were obtained from 1 inch thick plate stock. The composition of the 7075 alloy was 4.90 Zn, 2.64 Mg, 1.59 Cu, 0.31 Fe, 0.11 Si, 0.054 Mn, 0.20 Ti, 0.20 Cr. The composition of the 2024 alloy was 4.70 Cu, 1.72 Mg, 0.20 Si, 0.37 Fe, 0.60 Mn, 0.04 Zn, 0.10 Cr. The pure aluminum samples were cut from the interior of an ingot of 99.999 + % aluminum.

The specimens were wafers approximately 1.3 x 1 x 0.1 cm, and the wafers were polished and etched in one percent HF. The etching was followed by a distilled water rinse, a methanol rinse, and air drying at room temperature. As quickly as possible, specimens were then mounted on the spectrometer sample carousel and introduced into the vacuum chamber.

XPS/AES Analysis Parameters

Polished and etched aluminum specimens were examined in a physical Electronics Industries, Inc., (PEI) Model 548 XPS/AES spectrometer. A description of the experimental apparatus and the characteristics of the double-pass cylindrical mirror energy analyzer employed is available elsewhere (25). Typical base pressures in the sample vacuum chamber were in the range 10^{-8} - 10^{-9} torr.

All of the XPS spectra were obtained using a Mg K_{α} x-ray source operating at a voltage of 10 kV and a current of 40 MA. The electron multiplier voltage supply was 2 kV, and the analyzer response time was 20 msec. Wide XPS energy scans (1000 - 0 eV binding energy) were obtained at a scan rate of 3 eV/sec and a spectrometer energy analyzer pass energy of 100 eV. High resolution scans were obtained at a scan rate of 0.01 eV/sec and a pass energy of 50 eV. The time constant selected was a function of scan rate and photomultiplier sensitivity.

The XPS spectrometer binding energy scale was calibrated using the Au $4f_{7/2}$ photoelectron line from gold, which was found to be sharp and reproducible. Drift in the gold Au $4f_{7/2}$ line was negligible, (\pm 0.02 eV), and the binding energy of the peak was unaffected by argon ion sputtering. High resolution

scans of gold were obtained before and after each series of specimen examination. For all XPS spectra reported in this work, the reference level for the binding energy scale has been chosen to be zero at the Fermi level.

All AES spectra were obtained using an electron beam at a primary voltage of 5 kV and an emission current of 2 mA. Typical beam currents were 30 - 40 μ A, as measured by a Faraday cup. Typical electron multiplier voltage supply values were in the range 1.2 - 1.4 kV, and the energy analyzer response time was 5 msec. The spectrometer kinetic energy scale was calibrated by observation of a 2 kV elastic peak. The lock-in amplifier modulation was 3 volts peak-to-peak (VPP) at the low kinetic energy end of the spectrum, and 6 VPP at the high kinetic energy end. The time constant selected was a function of scan rate and lock-in amplifier sensitivity. Wide AES energy scans (0 - 2000 eV kinetic energy) were obtained at a scan rate of 7 eV/sec, and high resolution scans at a rate of 1 eV/sec.

Geometrical alignment of the sample specimen with the energy analyzer aperture was obtained by maximizing the 2 kV elastic peak signal in the AES mode. This alignment was accomplished as rapidly as possible in order to minimize any

possible electron beam damage to the specimen surface. Wide energy scan and high resolution XPS spectra were then obtained, followed by the acquisition of AES spectra.

Specimens were ion sputtered in an argon atmosphere at a pressure of 5×10^{-5} torr. The sputter gun voltage was 2 kV and the emission current 30 mA. The argon ion beam current was on the order of 0.01 μ A, as measured by a Faraday cup. Typical sputter times were 3 minutes. Multiplexed AES peak-to-peak height measurements were taken continuously during some of the ion sputterings to generate elemental concentration depth profiles, but XPS operation was not possible at such high sputtering pressures. The sample chamber was evacuated after ion sputtering, and first XPS spectra, then AES spectra, were obtained from the sputtered surfaces.

Notched cylindrical specimens, 1.5 mm diam. 12 mm long, with a notch depth of 0.25 mm, of 2024 and 7075 aluminum alloys were fractured in vacuo in a PEI Model 509A scanning Auger microscope (SAM). The anvil was chilled with liquid nitrogen to facilitate specimen fracture. The base pressure in the SAM system was $\sim 2 \times 10^{-10}$ torr. AES scans were obtained using a 5 kV primary electron excitation beam with an emission current of 0.15 mA and a beam current of 4 μ A, as

measured by a Faraday cup. The lock-in amplifier modulation was 3 VPP at the low kinetic energy end of the spectrum and 6 VPP at the high kinetic energy end. The electron multiplier voltage supply was in the range 0.7 - 0.9 kV. AES wide energy scans (0 - 2000 eV kinetic energy) were obtained at a rate of 7 eV/sec, and high resolution scans at a rate of 1 eV/sec. The kinetic energy scale was calibrated by observation of a 2 kV elastic peak. Low power (250x) secondary electron emission images of the fracture surfaces were also obtained.

XPS/AES Results

XPS wide energy scans (1000 - 0 eV binding energy of gold plated copper substrate reference standard specimens in the as-received condition exhibited high intensity carbon, C 1s, oxygen, O 1s and oxygen Auger signals, along with Au 4f and Au 4d signals and Cu 2p signals. After sputtering with argon ions the gold reference standards exhibited large increases in the Au 4d, Au 4f and Au 4p signal intensities, and Au 4s, Au 5p and Au 5d signals were also observable. The carbon, C 1s, signal from the argon-ion sputtered gold surfaces was strongly attenuated, and the oxygen, O, 1s signal was not observable. The gold Au 4f_{7/2} photoelectron line was observed to be sharp and reproducible. The intensity of the gold Au 4f_{7/2} line increased approximately sevenfold after argon ion sputtering, but the

binding energy of the peak remained constant. Representative wide scan (1000 - 0 eV binding energy) XPS spectra of gold in the as-received and argon-ion sputtered condition are shown in Figure 1. High resolution scans (89 - 82 eV binding energy) of the Au 4f_{5/2} and Au 4f_{7/2} regions of the XPS spectra from the gold reference standard specimen surfaces are shown in Figure 2.

In the XPS wide energy scans (1000 - 0 eV binding energy) of the pure aluminum, 2024 and 7075 aluminum alloy specimen surfaces, the signals of greatest absolute intensity were observed at binding energies corresponding to O 1s, C 1s and oxygen Auger transitions. Al 2p and Al 2s signals were observed in all of the specimens. The 2024 aluminum alloy specimens exhibited Cu 2p XPS signals, as did the 7075 alloy specimens, which also exhibited Zn 3p, Zn 3s and zinc Auger signals. Fluorine, F 1s, and fluorine Auger signals were observable in the XPS spectra of specimens which had been etched in HF. The intensity of XPS signals from carbon and oxygen contaminants decreased after argon ion sputtering, but C 1s, O 1s and oxygen Auger signals were still observable, even after repeated sputterings. Representative XPS wide energy scans (1000 - 0 eV binding energy) of pure aluminum and of 2024 and 7075 aluminum alloy specimen surfaces in the argon ion sputtered condition are shown in Figure 3.

AES wide energy scans (0 - 2000 eV kinetic energy) of the pure aluminum and 2024 and 7075 aluminum alloy specimen surfaces were characterized by strong oxygen, carbon and aluminum oxide signals, as indicated by peak position (1381 - 1385 eV kinetic energy) and characteristic line shape (in the derivative mode spectrum). Argon and sulphur signals were also detectable. Copper signals were observable in the AES spectra of 2024 and 7075 aluminum alloy specimens. Zinc signals were observable in the 7075 alloy specimens. Fluorine signals were observable in the AES spectra of specimens which had been etched in HF. Representative AES wide energy scans (0 - 2000 eV kinetic energy) of pure aluminum and of 2024 and 7075 commercial aluminum alloy specimen surfaces are shown in Figures 4, 5 and 6, respectively. High resolution scans of the aluminum KLL region of the AES spectra (1275 - 1475 eV kinetic energy) of pure aluminum, and of 2024 and 7075 aluminum alloy specimen surfaces in the polished condition are shown in Figure 7.

High Resolution XPS Spectra

Doublet peaks were observed in the Al 2p and Al 2s regions of the high resolution XPS spectra of pure aluminum and 2024 and 7075 aluminum alloy specimen surfaces. Heavily oxidized specimens in the as-received or polished condition were characterized by a single XPS Al 2p peak, with a barely

detectable "shoulder" on the low binding energy side. This Al 2p peak was centered at 75.8 ± 0.2 eV on the binding energy scale, referred to the Fermi level, with a full width at half maximum (FWHM) of ~ 2.5 eV. After prolonged argon ion sputtering of the sample surfaces, a single Al 2p peak was observed centered at 72.6 ± 0.2 eV, with a shoulder on the high binding energy side. A doublet in the Al 2p region with component peaks separated by 3.2 ± 0.2 eV was observable in the XPS spectra of specimens which had been ion sputtered for an intermediate duration and/or which had been previously HF etched.

The Al 2s peak in the high resolution XPS spectra characteristic of the oxidized pure aluminum and 2024 and 7075 aluminum alloy specimen surfaces was centered at 120.5 ± 0.5 eV and the Al 2s peak characteristic of specimen surfaces which had received a prolonged argon ion sputtering was centered at 118.0 ± 0.2 eV. Etched and/or argon ion sputtered specimens exhibited both Al 2s peak components, separated by ~ 2.5 eV. Representative high resolution scans of the Al 2p region (85 - 65 eV binding energy) and the Al 2s region (130 - 110 eV binding energy) of the XPS spectra of specimen surfaces in the polished, HF etched and argon ion sputtered condition are shown in Figures 8, 9 and 10 for pure aluminum and for 2024 and 7075 commercial aluminum alloys,

The doublet structure in the Al 2p and Al 2s regions of the XPS spectra shown in Figures 8-10 demonstrates the existence of aluminum in two distinct chemical states. XPS spectra obtained from polished aluminum specimen surfaces exhibited only Al 2p and Al 2s peaks characteristic of aluminum oxide, centered at 75.8 and 120.5 eV binding energy, respectively. Subsequent surface cleaning treatments revealed Al 2p and Al 2s peaks characteristic of metallic aluminum, centered at 72.6 and 118.0 eV binding energy, respectively, which increased in intensity with further argon ion sputtering.

Oxygen: High Resolution XPS Spectra

Small shifts in the oxygen, O, 1s peak positions were observed in the high resolution XPS spectra of the aluminum specimens. Specimens in the as-received or polished condition were characterized by an oxygen, O, 1s peak centered at a binding energy of 533.1 ± 0.2 eV (FWHM ~ 3.8 eV). The oxygen, O, 1s peak from specimens which had received a prolonged argon ion sputtering was centered at 531.0 ± 0.4 eV (FWHM ~ 3.2 eV). Specimens which had been etched and/or partially sputtered exhibited oxygen, O, 1s peaks within this range of binding energy values. The oxygen, O, 1s, peaks appeared to be smooth and Gaussian, and additional peak structure was not detected. Representative XPS high resolution scans of the oxygen, O 1s, region (560 - 520 eV binding energy) of specimen surfaces in the polished, HF etched and argon ion

sputtered condition are shown in Figures 11, 12 and 13 for pure aluminum and for 2024 and 7075 alloys, respectively.

Representative high resolution scans of the oxygen, $O 1s$, region (560 - 520 eV binding energy) of the XPS spectra of the surfaces of specimens of gold, pure aluminum, and 2024 and 7075 commercial aluminum alloys in the polished or as-received condition are shown in Figure 14.

Aluminum Fracture Surfaces: SAM Spectra

Aluminum specimens which had been chilled in liquid nitrogen and fractured in vacuo at $\sim 2 \times 10^{-10}$ torr in the SAM system were much less contaminated than any of the aluminum specimens cleaned in situ in the XPS/AES system. SAM spectra obtained from the surfaces of 2024 and 7075 aluminum alloy specimens fractured in vacuo differed significantly from AES spectra obtained from sputtered aluminum surfaces. SAM spectra of aluminum fracture surfaces were characterized by extremely weak oxygen signals and strong aluminum signals characteristic of metallic aluminum, as indicated by the aluminum KLL peak positions (1392 - 1395 eV kinetic energy) and characteristic line shape (in the derivative mode spectrum), whereas the corresponding AES spectra of sputtered aluminum surfaces were characterized by strong contaminant signals and aluminum KLL signals with characteristic aluminum oxide line shape and

peak positions (1385 - 1389 eV kinetic energy). SAM wide energy scans (0 - 2000 eV kinetic energy) of the surfaces of 2024 and 7075 aluminum alloy specimens fractured in vacuo are shown in Figures 15 and 16, respectively. High resolution scans of the aluminum KLL region of the SAM spectra (1275 - 1475 eV kinetic energy) of fracture surfaces of 2024 and 7075 commercial aluminum alloys are shown in Figure 17.

The electron emission spectrum obtained from the surface of a 2024 aluminum alloy specimen fractured in vacuo exhibited characteristic energy loss peaks (separated by ~ 15.7 eV), observed near the 2 kV elastic peak during calibration of the SAM spectrometer energy analyzer. Characteristic energy loss peaks (due to bulk plasmon excitations (26, 27) in the high resolution true secondary electron emission spectrum (1825 - 2025 eV kinetic energy) of the fracture surface of a 2024 commercial aluminum alloy specimen are shown in Figure 18.

Specimens in Water-Vapor-Saturated Air

Wafer specimens were exposed to 24 hours in water vapor saturated air, at 70°C, following the procedures described by Scamans and Tuck (23). The surfaces were dried in methanol and then analyzed by XPS and SAM. In Figures 19, 20 and 21 we compare the Al 2s and Al 2p lines for surfaces which had

been polished (this was the starting condition) with surfaces which had been exposed and then subsequently cleaned by argon-ion bombardment. It is evident that the lines have been broadened by the water vapor exposure and the shift of the most prominent peaks suggests that oxides or hydroxides have formed. The water vapor exposures resulted in much broader peaks than exposure to dry air and this may be characteristic of the hydroxides.

SAM spectra for the 2024 and 7075 alloys are shown in Figure 22 and 23. The shifts in the Al KLL lines are approximately 10 eV, and these are close to those observed for specimens exposed to dry air (Figure 7). Only the shifted aluminum peaks were observed in these spectra since AES is sensitive only to surface structures.

Notched cylindrical specimens were also exposed to water-vapor-saturated air at 70°C for 24 hours. These were then fractured at liquid nitrogen in the apparatus at 10^{-10} and examined by SAM. The center of the fracture area exhibited the clean AES spectra shown in Figures 22 and 23 and the cylindrical areas the shifted lines shown in the same figure. An attempt was then made to obtain spectra close to the base of the notch at grain boundary intersections. On the whole, most of the spectra were those of the clean aluminum. Occasionally, peaks with small shifts were observed, but these were judged to be caused by contamination which

occurred by smearing of the edges. We had anticipated that grain boundary regions close to the surface would show shifts in the aluminum lines which would indicate that oxygen had penetrated the grain boundaries and that the embrittlement was associated with an internal oxidation. Our data were inconclusive on this point. The specimens exposed to water vapor fractured very easily in comparison with fresh specimens but we were unable to specify the mechanism of embrittlement.

SUMMARY AND CONCLUSIONS

Aluminum was found to exist in two chemical states at the surfaces of pure aluminum, 2024 and 7075 aluminum alloys. The observed line shape of the principal aluminum KLL peaks in the AES spectra of aluminum specimen surfaces in the polished or argon-ion sputtered condition was characteristic of aluminum oxide (Fig. 7), whereas the KLL line shape in the AES spectra obtained from aluminum alloy fracture surfaces was characteristic of metallic aluminum (Fig. 17). These characteristic AES spectra agreed with reference spectra obtained by Davis, et al (28).

The Al 2p region of the XPS spectra obtained from pure aluminum and from 2024-T351 and 7075-T651 commercial aluminum alloy surfaces exhibited either single peaks with observable peak structure or a doublet with two distinct peak components,

separated by ~ 3.2 eV (Figs. 8-10). The relative intensities of the two doublet peak components varied as a function of specimen history. The Al 2p peak centered at 72.6 ± 0.2 eV binding energy is characteristic of electronic transitions involving energy-levels in atoms surrounded by the bulk metallic environment, whereas the aluminum Al 2p peak centered at 75.8 ± 0.2 eV binding energy corresponds to energy-levels in aluminum ions in the oxide phase, as indicated by the observation that specimen surfaces which had been only partially etched and/or partially argon-ion sputtered demonstrated both XPS Al 2p signals, separated by a chemical shift of ~ 3.2 eV. Repeated argon-ion sputtering resulted in a decrease in the intensity of the XPS signal contribution from the oxide phase with a simultaneous increase in the intensity of the XPS signal contribution from atoms in the metallic environment.

This assignment of characteristic binding energies of XPS spectral features to the oxidation states of the emitting species is in agreement with Farrell (29), who noted the existence of doublet aluminum Al 2p peaks, attributed to contributions from ions in the oxide, and from atoms in the bulk metal. The observation of the metallic aluminum Al 2p peak centered at 72.6 ± 0.2 eV binding energy is in good agreement with the value of 73.0 ± 0.1 eV binding energy

given by Flodstrom, et al (30), and with the value of 72.65 eV binding energy observed in XPS reference spectra recently obtained by Wagner, et al (31). The magnitude of the ~ 3.2 eV chemical shift observed agrees with the observation by Eberhardt and Kunz (32) of peak structure in a region of up to 3 eV higher binding energies than the metallic Al 2p peak. Heavily oxidized aluminum surfaces would be expected to exhibit larger chemical shifts between the oxide and bulk metal XPS peaks than the chemical shifts observed in the early stages of the oxidation of clean aluminum surfaces.

Doublet peak structure, previously unreported, was observed in the aluminum Al 2s region of the XPS spectra obtained from pure aluminum and from commercial aluminum alloy specimen surfaces. Oxidized specimen surfaces were characterized by a single Al 2s peak centered at 120.5 ± 0.5 eV binding energy. Argon ion sputtered specimen surfaces were characterized by a single aluminum Al 2s peak centered at 118.0 ± 0.2 eV binding energy. Aluminum specimen surfaces partially sputtered exhibited a doublet with two peak components, separated by a chemical shift of ~ 2.5 eV (Figs. 8-10).

Contaminant species could not be completely eliminated from the cleaned specimen surfaces, as indicated by SAM spectra from fracture surfaces, and by AES spectra and XPS spectra (Fig. 3) obtained from argon ion sputtered specimens.

AES spectra obtained from all of the aluminum specimens in the argon ion sputtered condition still exhibited signals with Al KLL Auger line shape characteristic of aluminum oxide (Fig. 7). Only specimens fractured in the SAM system exhibited Auger spectra with the Al KLL line shape characteristic of metallic aluminum (Fig. 17). XPS oxygen, O 1s, signals centered at 531.0 ± 0.4 eV binding energy, characteristic of alumina (34, 31, 33), were present in the spectra obtained from all of the aluminum specimen surfaces, even after a prolonged argon ion sputtering (Figs. 11-13). Specimens in the polished or as-received condition exhibited XPS oxygen O 1s signals centered at 533.1 ± 0.2 eV binding energy (Fig. 14), characteristic of a hydroxide phase, or of a combination of an oxide phase and adsorbed water (34). Characteristic energy loss peaks in the true secondary electron emission spectrum from aluminum surfaces were observed only from fracture surfaces in the SAM system. This characteristic loss spectrum indicated a lack of contaminant species on the fracture surface, since this spectrum is extremely sensitive to surface conditions. The bulk plasmon loss peaks near the 2 kV elastic peak were separated by ~ 15.7 eV, in good agreement with the value of 15.5 eV observed by Pillon, et al (26) using a primary beam energy of 0.8 kV.

Our attempts to find grain boundary oxidation of aluminum using SAM scans near the surface of aluminum alloys embrittled by exposure to water-vapor-saturated air at 70°C for 24 hours were inconclusive. There were slight shifts in the KLL Auger spectra at some grain boundary intersections with the surface, but the resolution was inadequate to allow definitive observation.

ACKNOWLEDGEMENTS

The author would like to acknowledge the extensive experimental work of M. J. Ralph. Much of the early data were obtained in the course of his work toward the S.M. degree. We would also like to acknowledge the assistance of Dr. Anthony Garrett-Reed, and Mr. P. P. Kelleher.

This work was sponsored by the Air Force Office of Scientific Research under Grant AFOSR 76-2924B and the interest of Major Wilbur C. Simmons was greatly appreciated.

REFERENCES

1. W.H. Kreuger and S.R. Pollack, *Surface Sci.* 30 (1972) 263.
2. C.T. Kirk, Jr. and E.E. Huber, Jr., *Surface Sci.* 9 (1968) 217.
3. G. Dorey, *Surface Sci.* 27 (1971) 311.
4. W.H. Krueger and S.R. Pollack, *Surface Sci.* 30 (1972) 280.
5. E.E. Huber, Jr. and C.T. Kirk, Jr., *Surface Sci.* 5 (1966) 447.
6. E.E. Huber, Jr. and C.T. Kirk, Jr., *Surface Sci.* 8 (1967) 458.
7. T. Fort, Jr. and R.L. Wells, *Surface Sci.* 32 (1972) 543.
8. J.A. Ramsey, *Surface Sci.* 8 (1967) 313.
9. J.K. Grepstad, P.O. Gartland and B.J. Slagsvold, *Surface Sci.* 57 (1976) 348.
10. P.O. Gartland, *Surface Sci.* 62 (1977) 183.
11. P.H. Dawson, *Surface Sci.* 57 (1976) 229.
12. M. Gettings and J.P. Coad, *Surface Sci.* 53 (1975) 636.
13. T. Smith, *Surface Sci.* 55 (1976) 601.
14. C. Benndorf, H. Seidel and F. Thieme, *Surface Sci.* 67 (1977) 469.
15. F. Jona, *J. Phys. Chem. Solids*, 28 (1967) 2155.
16. H. Shimizu, M. Ono and K. Nakayama, *Surface Sci.*, 36 (1973) 817.
17. K.S. Kim, W.E. Baitinger, J.W. Amy and N. Winograd, *J. Electron Spectrosc.* 5 (1974) 351.
18. I.M. Ritchie and G.L. Hunt, *Surface Sci.* 15 (1969) 524.
19. J.E. Boggio, *Surface Sci.*, 14 (1969) 1.
20. J.S.L. Leach, *Surface Sci.* 53 (1975) 257.

21. J.C. Grosskreutz, *Surface Sci.* 8 (1967) 173.
22. G.G. Garrett and J.F. Knott, *Acta Met.* 23 (1975) 841.
23. G.M. Scamans and C.D.S. Tuck, *International Conference on Mechanisms of Environment Sensitive Fracture of Materials*, Metals Society (1977) Guildford.
24. G.M. Scamans, R. Alani and P.R. Swann, *Corros. Sci.* 16 (1976) 443.
25. P.W. Palmberg, *J. Electron Spectrosc.* 5 (1974) 691.
26. J. Pillon, D. Roptin and M. Cailler, *Surface Sci.* 59 (1976) 741.
27. H. Raether, *Surface Sci.* 8 (1967) 233.
28. L.E. Davis et al., Handbook of Auger Electron Spectroscopy, Physical Electronic Industries, Inc., Eden Prairie, Minn.
29. T. Farrell, *Metal Science* 10 (1976) 87.
30. S.A. Flodstrom, R.Z. Bachrach, R.S. BAuer and S.B.M. Hagstrom, *Phys. Rev. Lett.* 37 (1976) 1282.
31. C.D. Wagner, et al al., Handbook of X-Ray Photoelectron Spectroscopy, Physical Electronics Industries, Inc., Eden Prairie, Minn.
32. W. Eberhardt and C. Kunz, *Surface Sci.* 75 (1978) 709.
33. D.M. Hercules, *Private Communication*, 18 Jan. 1979.
34. J.C. Fuggle, L.M. Watson, D.J. Fabian, and S. Affrossman, *Surface Sci.* 49 (1975) 61.

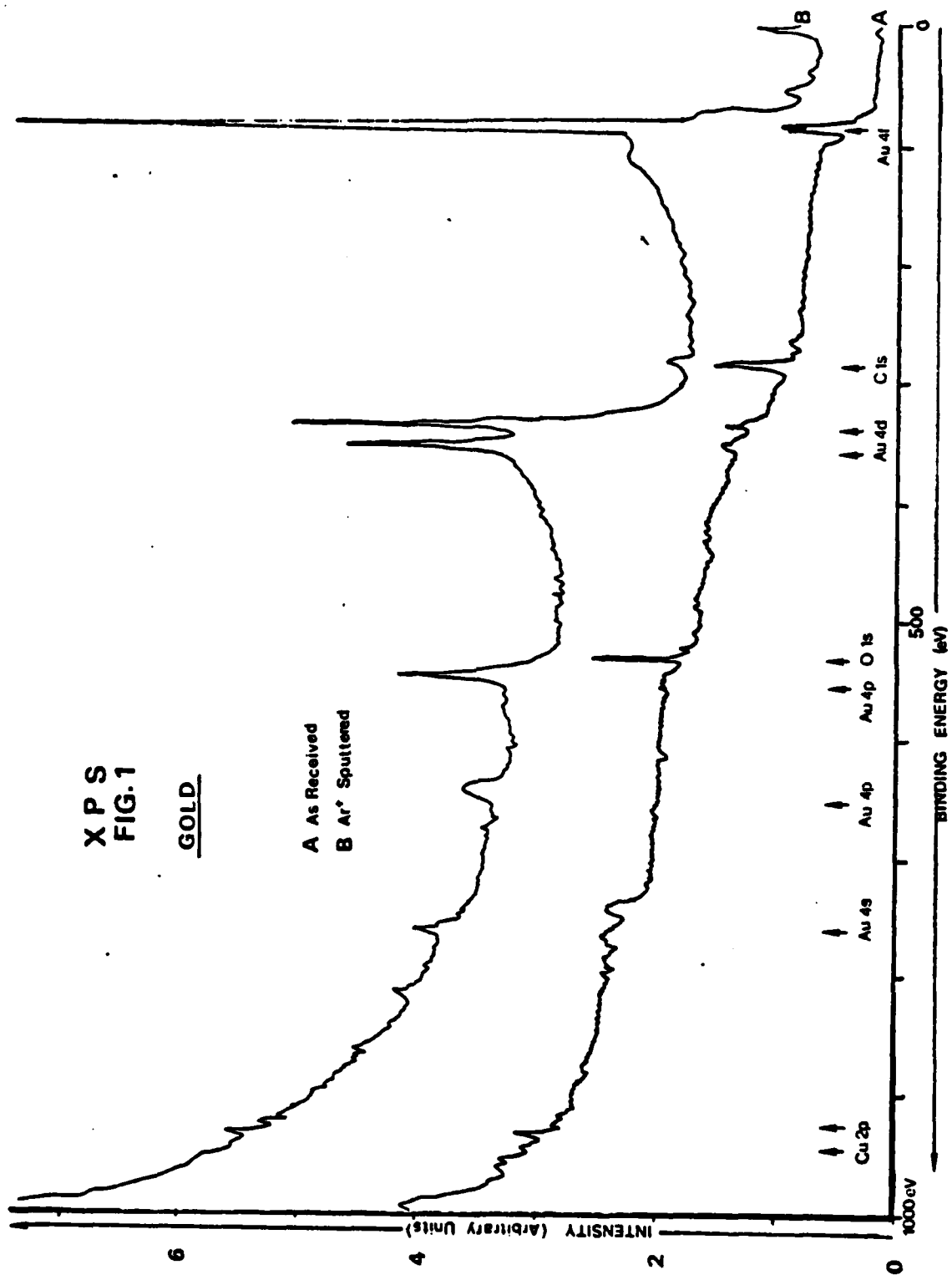


Figure 1. Gold: XPS Wide Scan Spectra

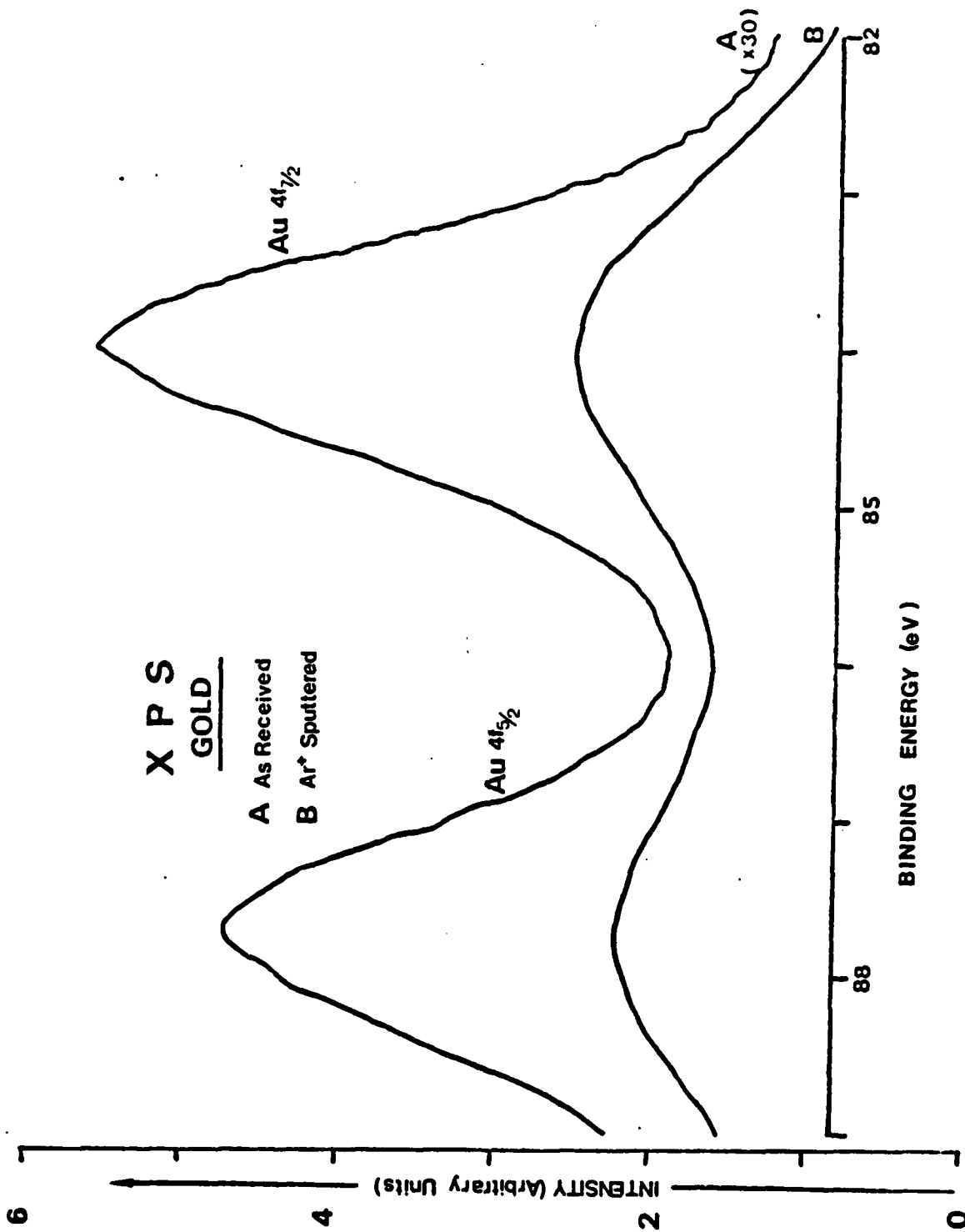


Figure 2. Gold: XPS High Resolution Spectra (Au 4f_{5/2} & Au 4f_{7/2} Regions)

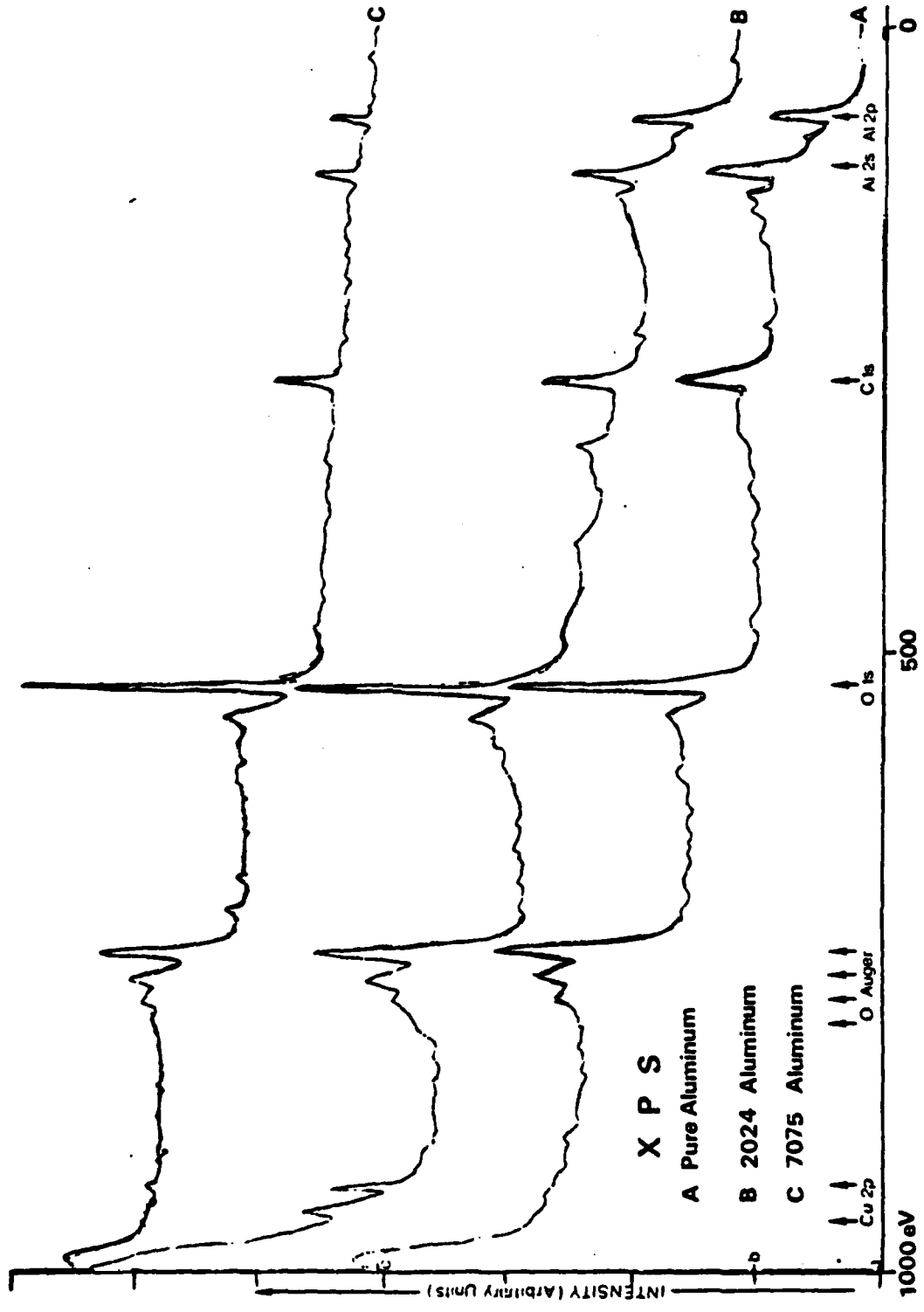


Figure 3. Aluminum: XPS Wide Scan Spectra

A E S
PURE ALUMINUM

FIG. 4

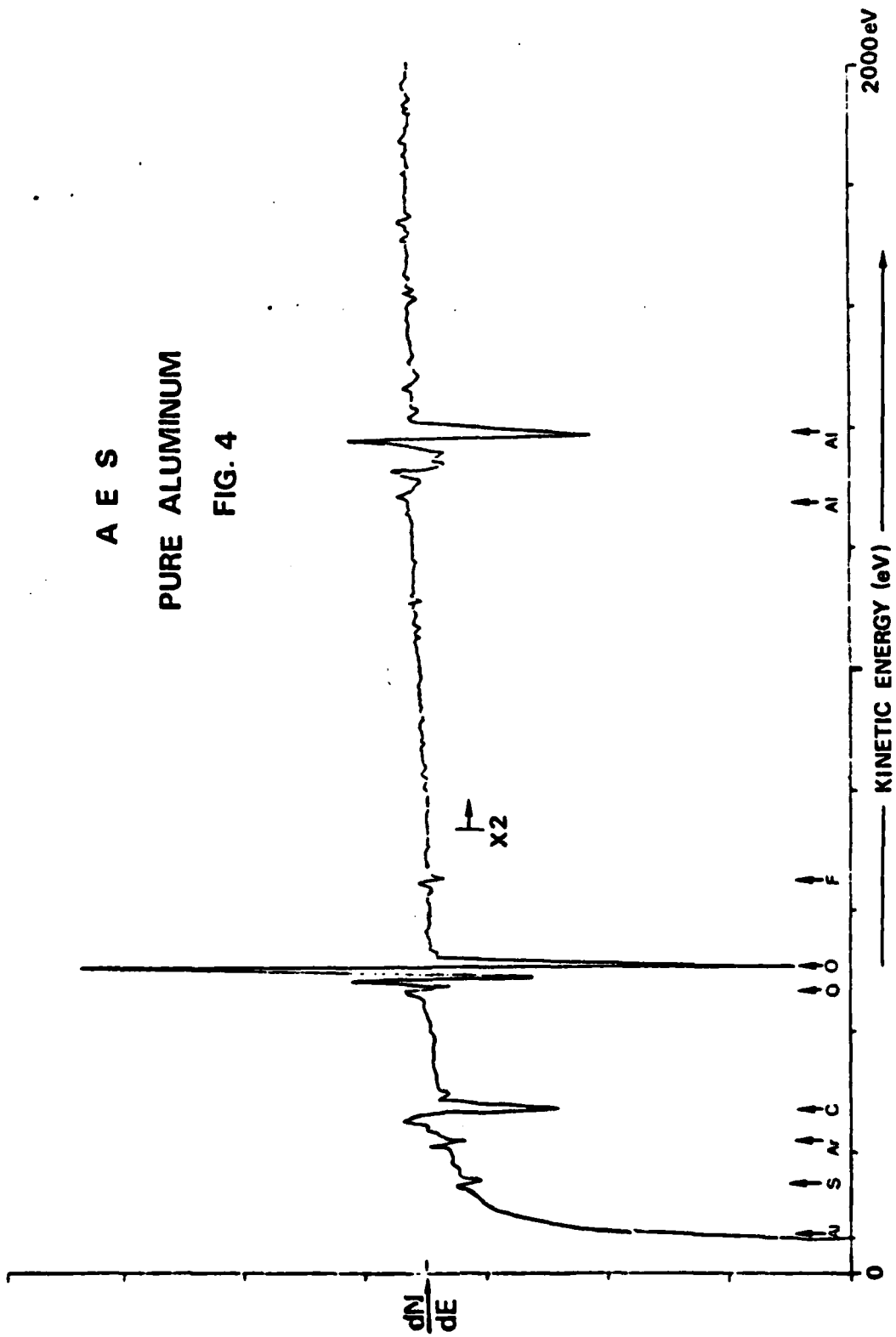


Figure 4. Pure Aluminum: AES Wide Scan Spectrum

A E S

2024 ALUMINUM

FIG. 5

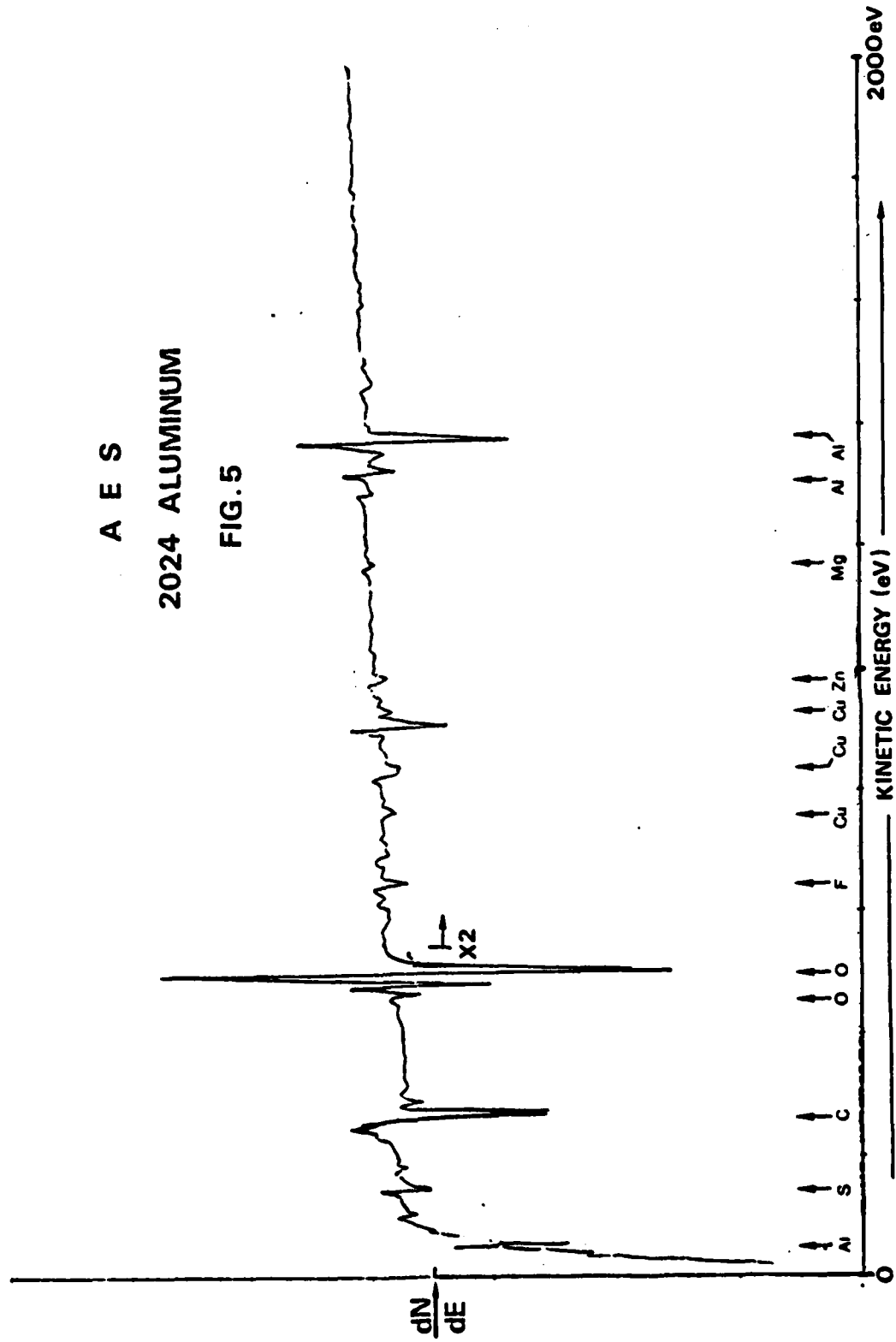


Figure 5. 2024-T351 Aluminum: AES Wide Scan Spectrum

A E S
7075 ALUMINUM

FIG. 6

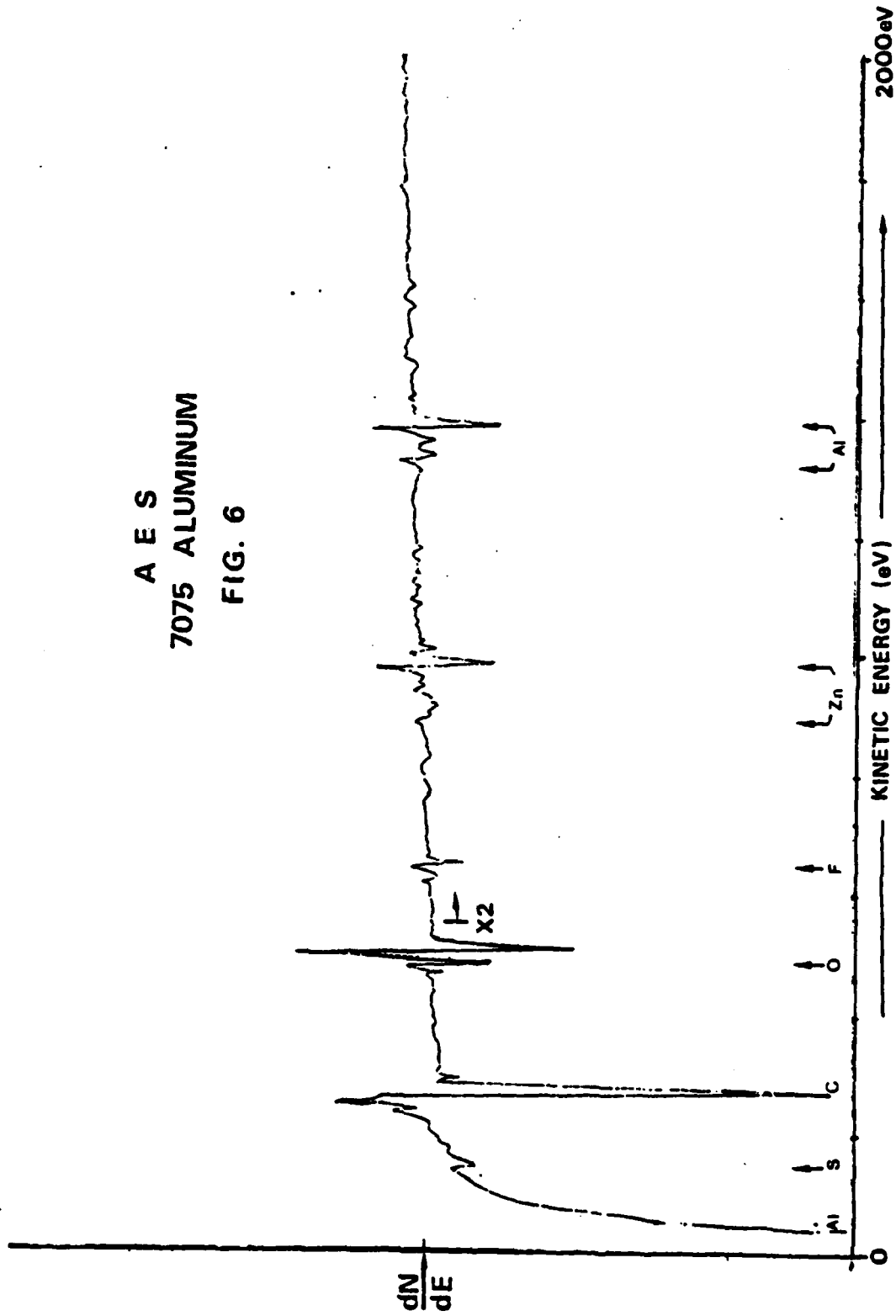


Figure 6. 7075-T651 Aluminum: AES wide scan Spectrum

AES
FIG. 7

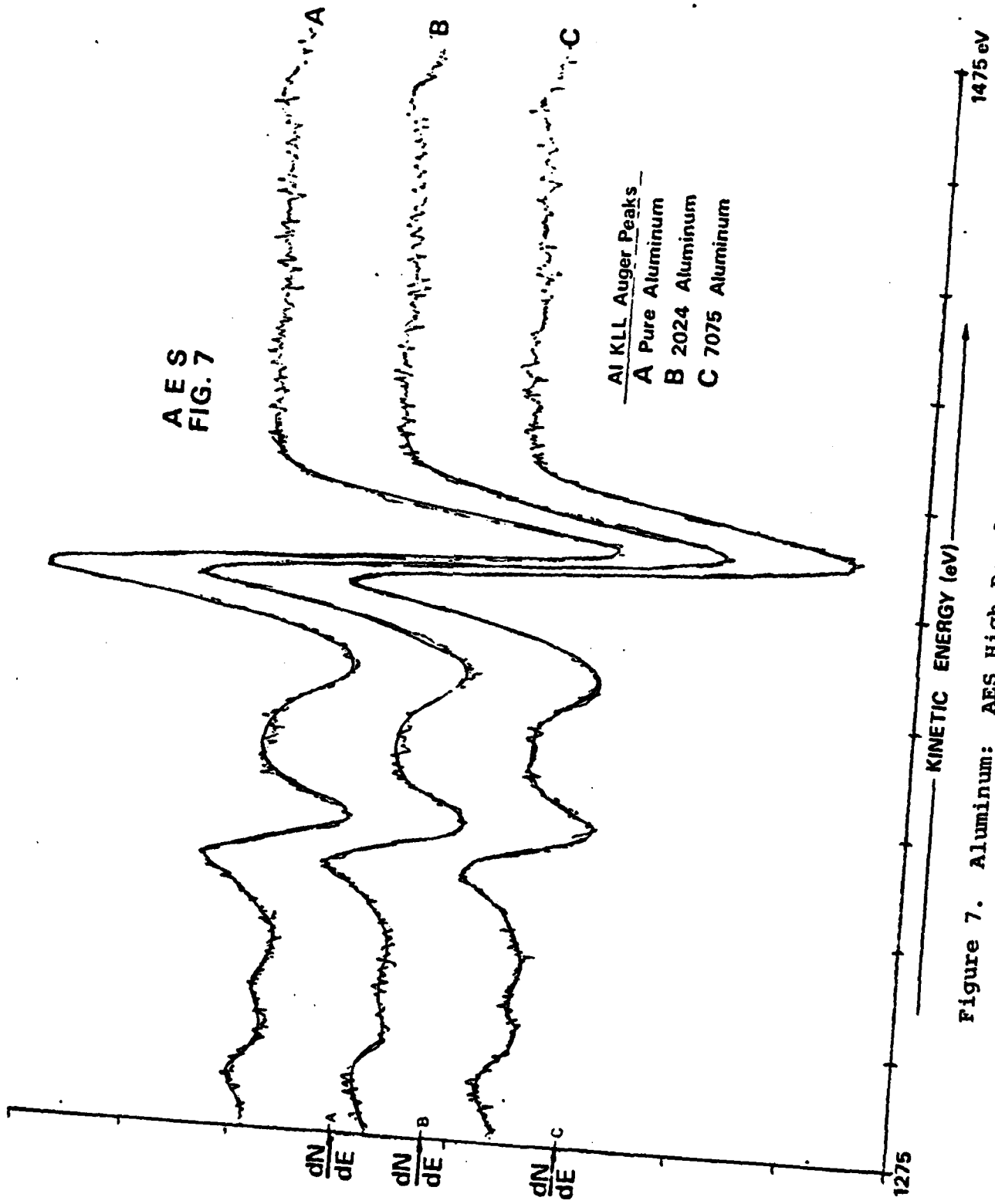


Figure 7. Aluminum: AES High Resolution Spectra

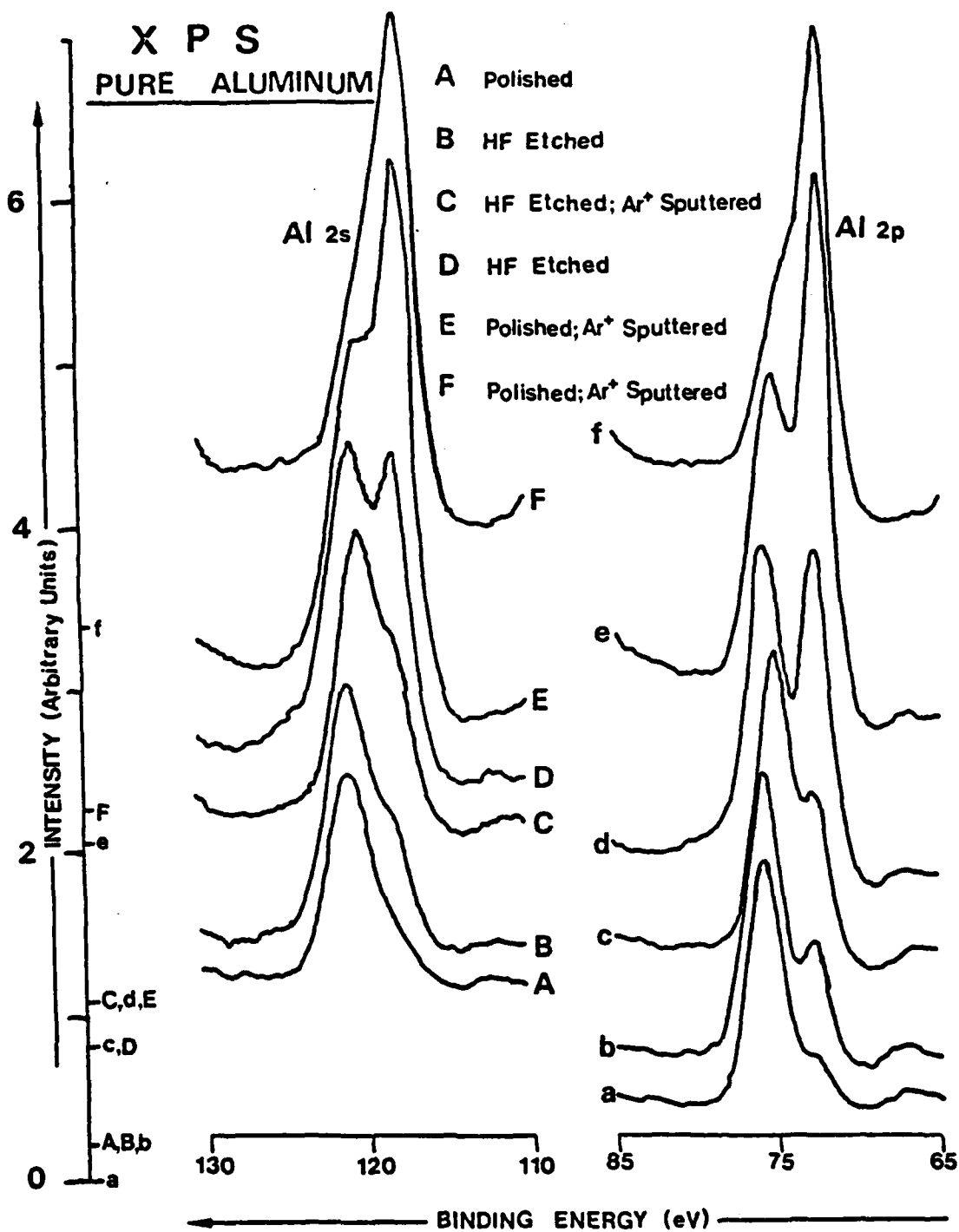


FIG. 8

Figure 8. Pure Aluminum: XPS High Resolution Spectra (Aluminum Al 2p & Al 2s Regions)

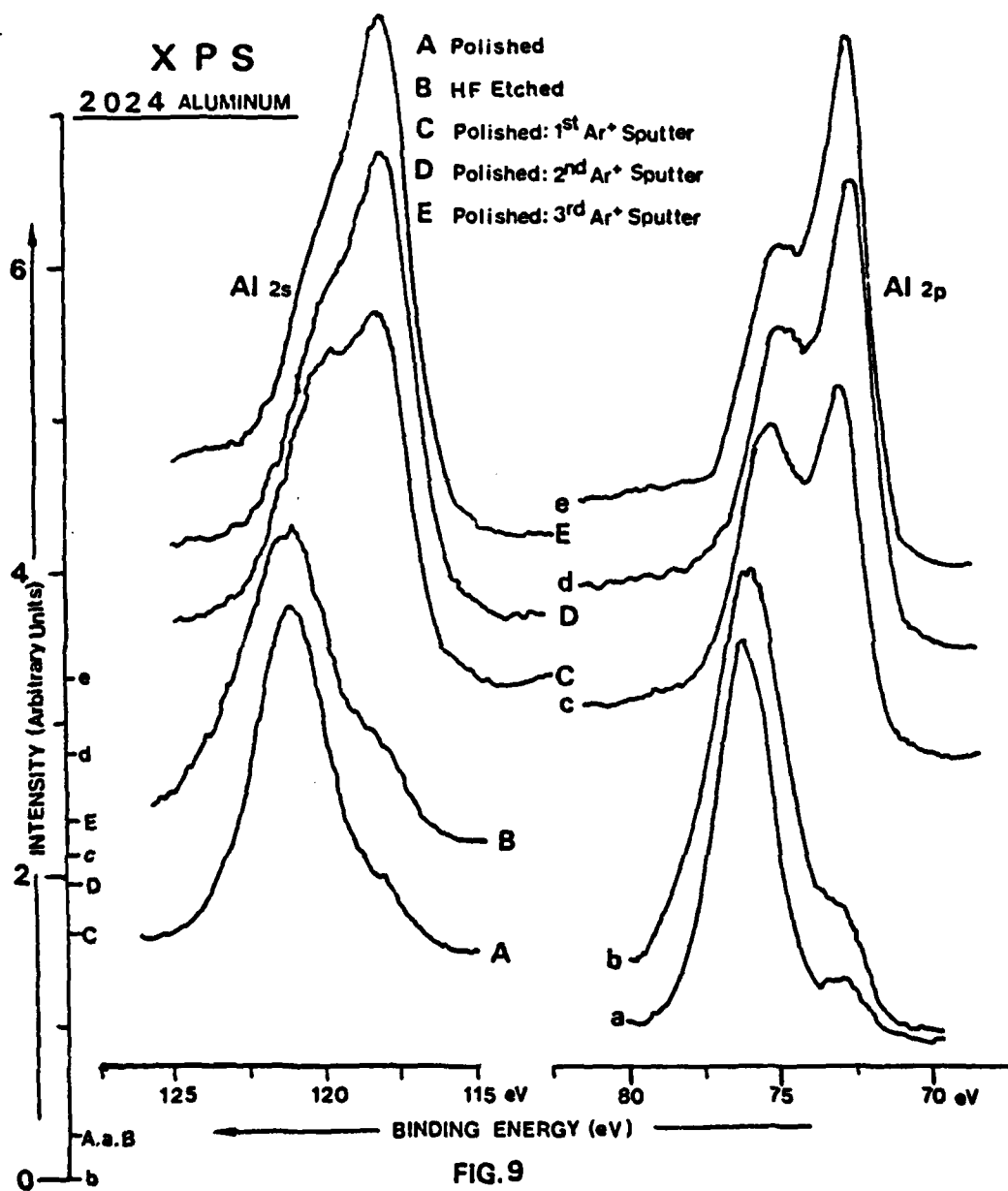


Figure 9. 2024-T351 Aluminum: XPS High Resolution Spectra (Aluminum Al 2p & Al 2s Regions)

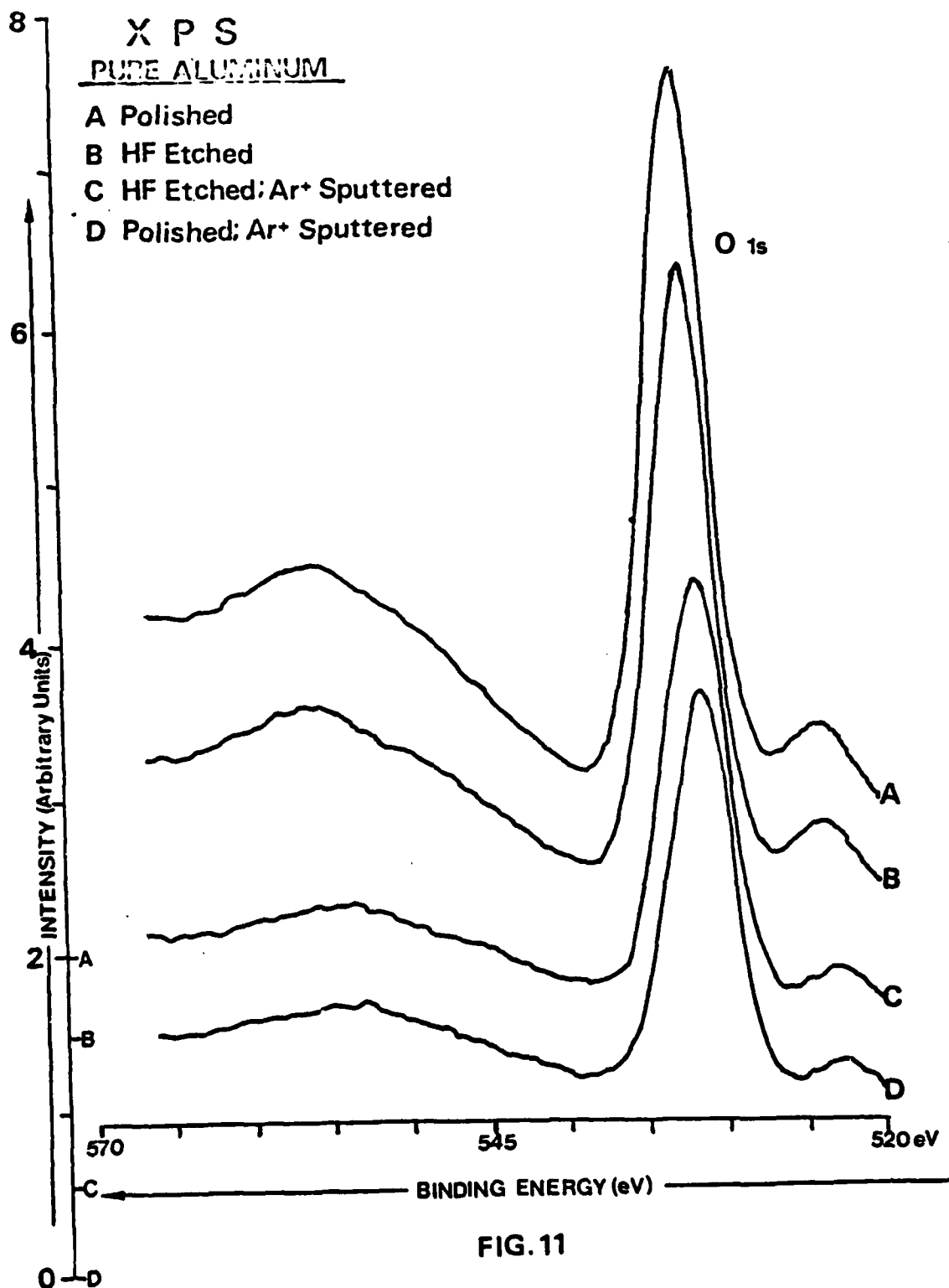


Figure 11. Pure Aluminum: XPS High Resolution Spectra (Oxygen O 1s Region)

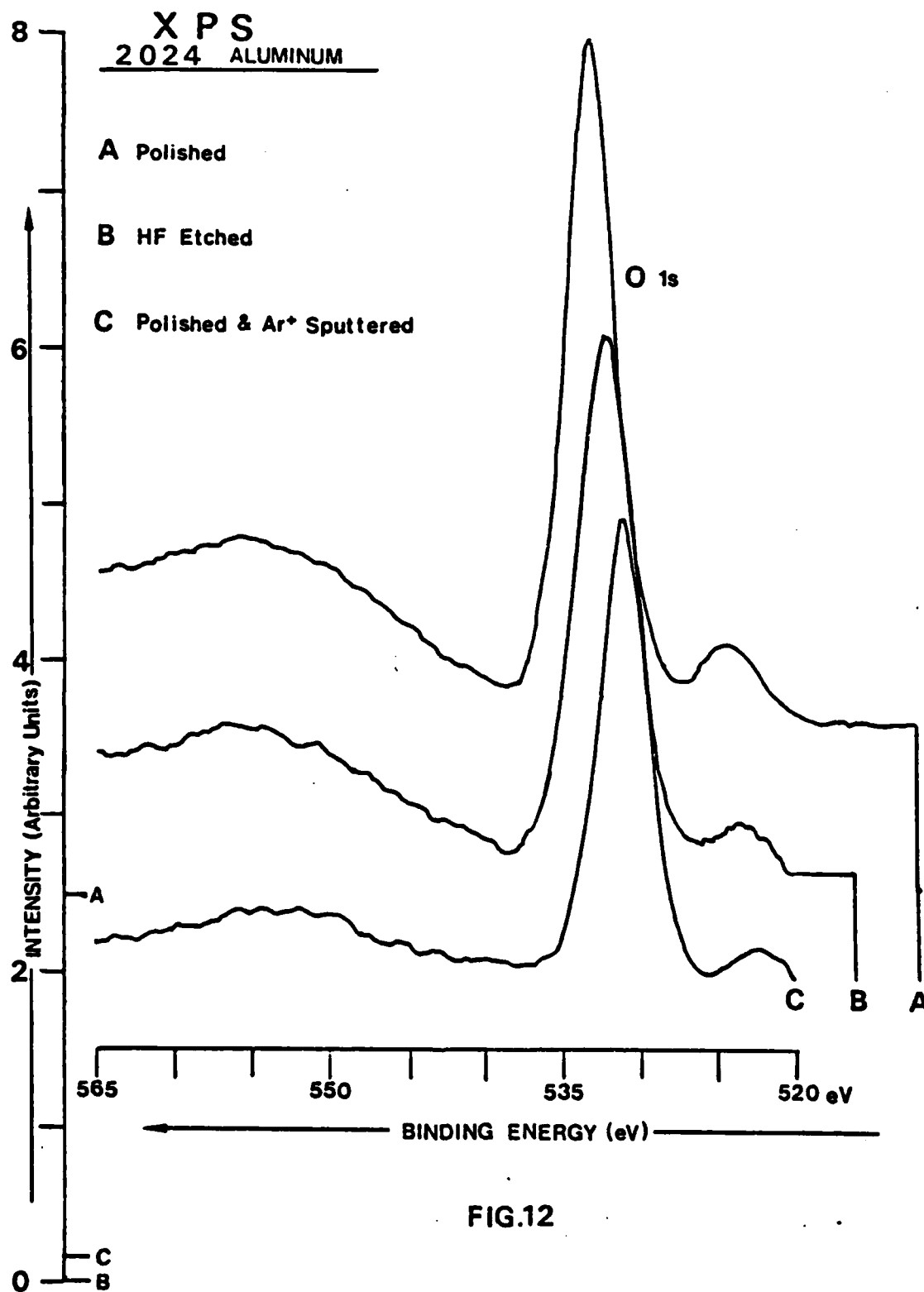


Figure 12. 2024-T351 Aluminum: XPS High Resolution Spectra (Oxygen O 1s Region)

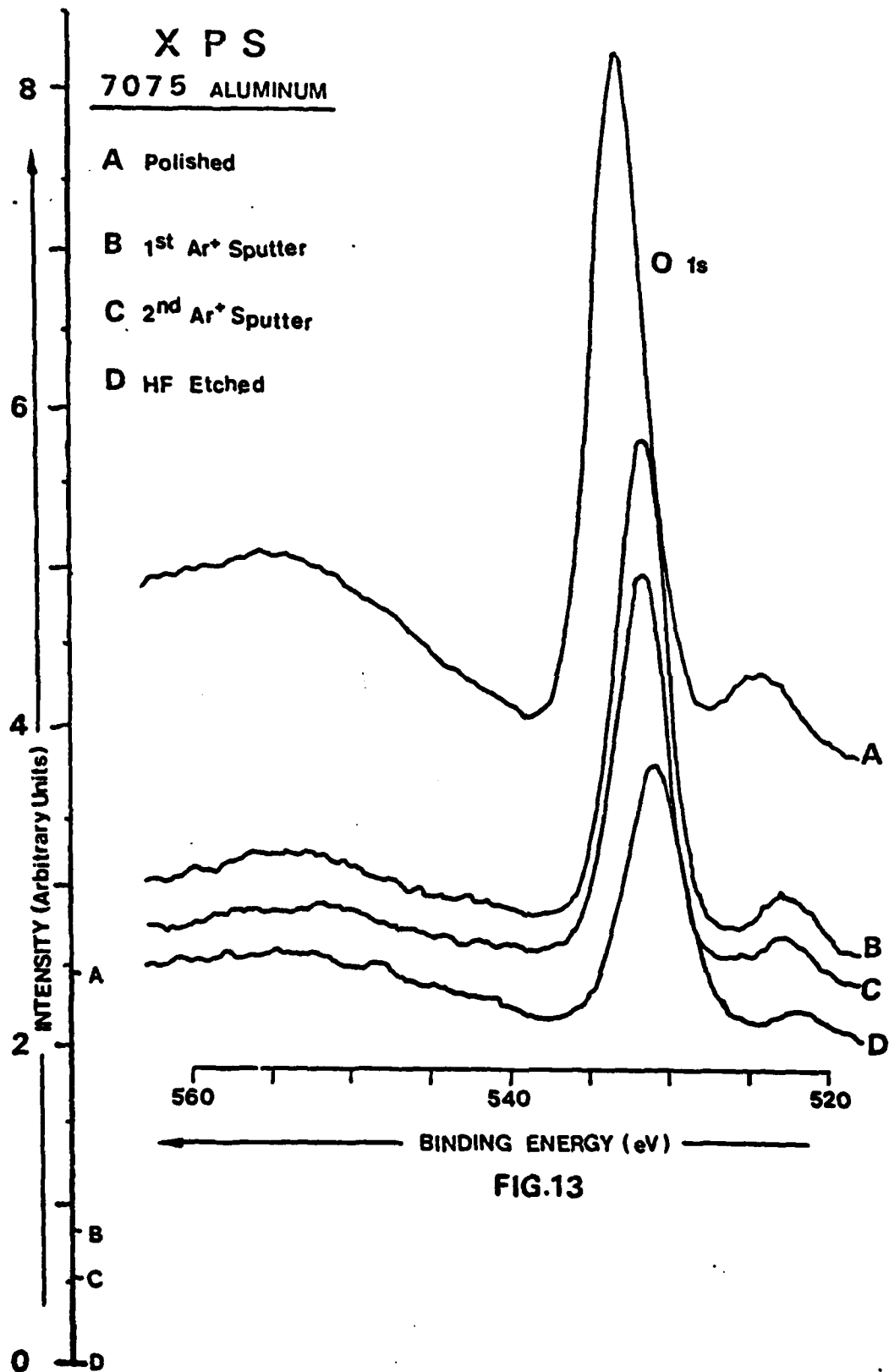


Figure 13. 7075-T651 Aluminum: XPS High Resolution Spectra (Oxygen O 1s Region)

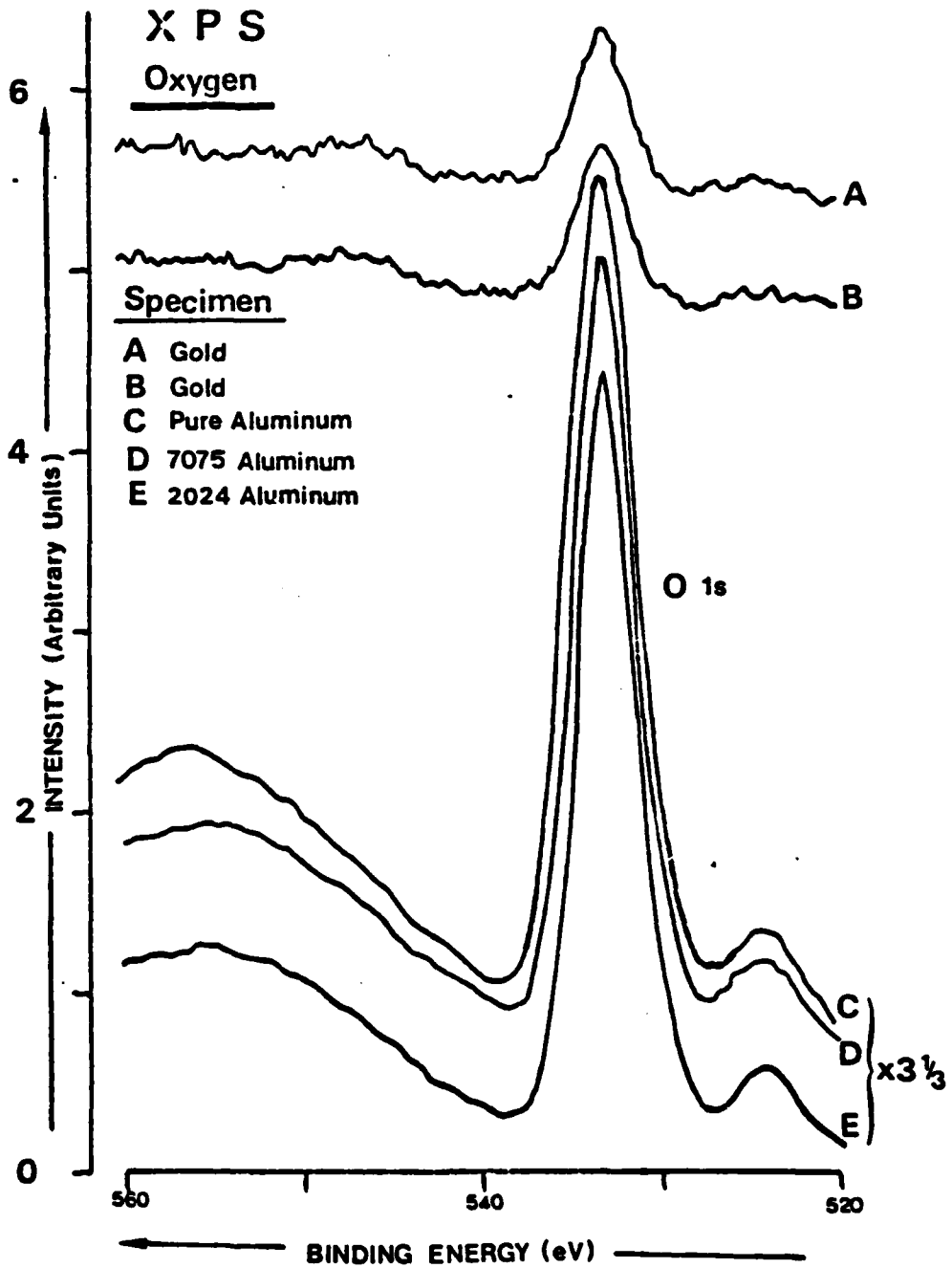


FIG.14

Figure 14. Gold & Aluminum: XPS High Resolution Spectra (Oxygen O 1s Region)

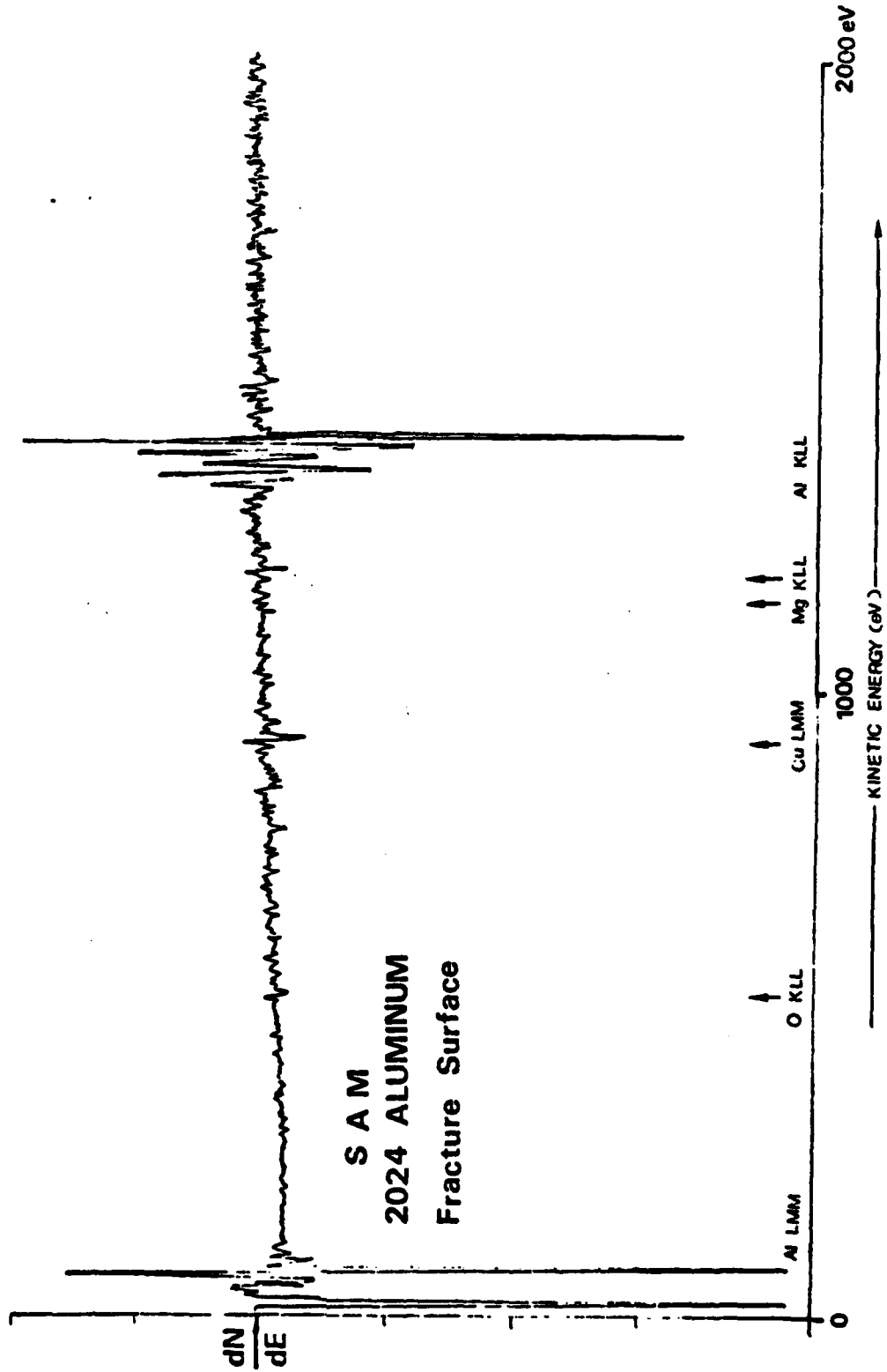
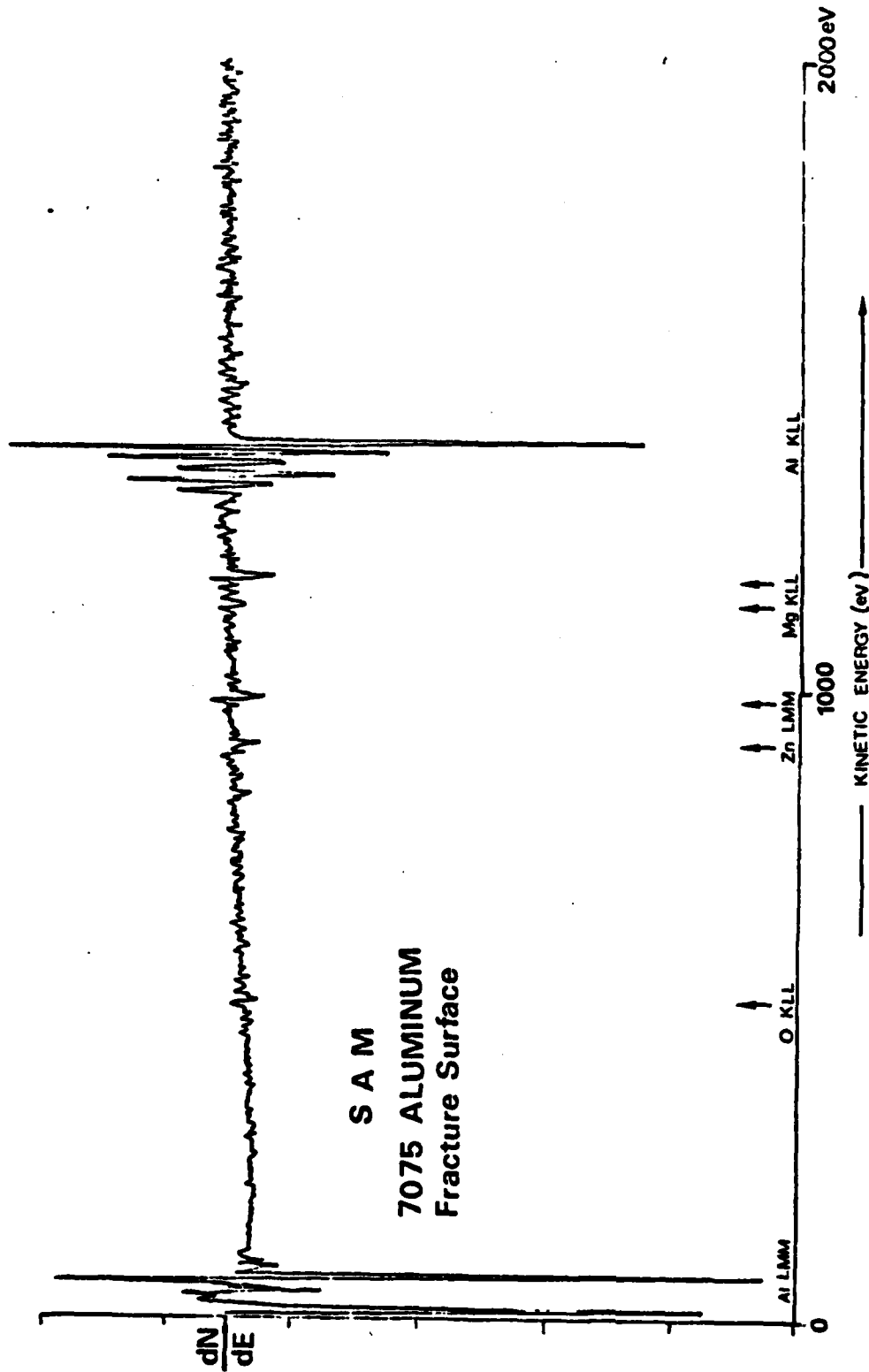


FIG. 15

Figure 15. 2024-T351 Aluminum Fracture Surface: SAM Wide Scan Spectrum



S A M
 7075 ALUMINUM
 Fracture Surface

FIG. 16

Figure 16. 7075-T651 Aluminum Fracture Surface: SAM Wide Scan Spectrum

S A M
FRACTURE SURFACES

FIG. 17

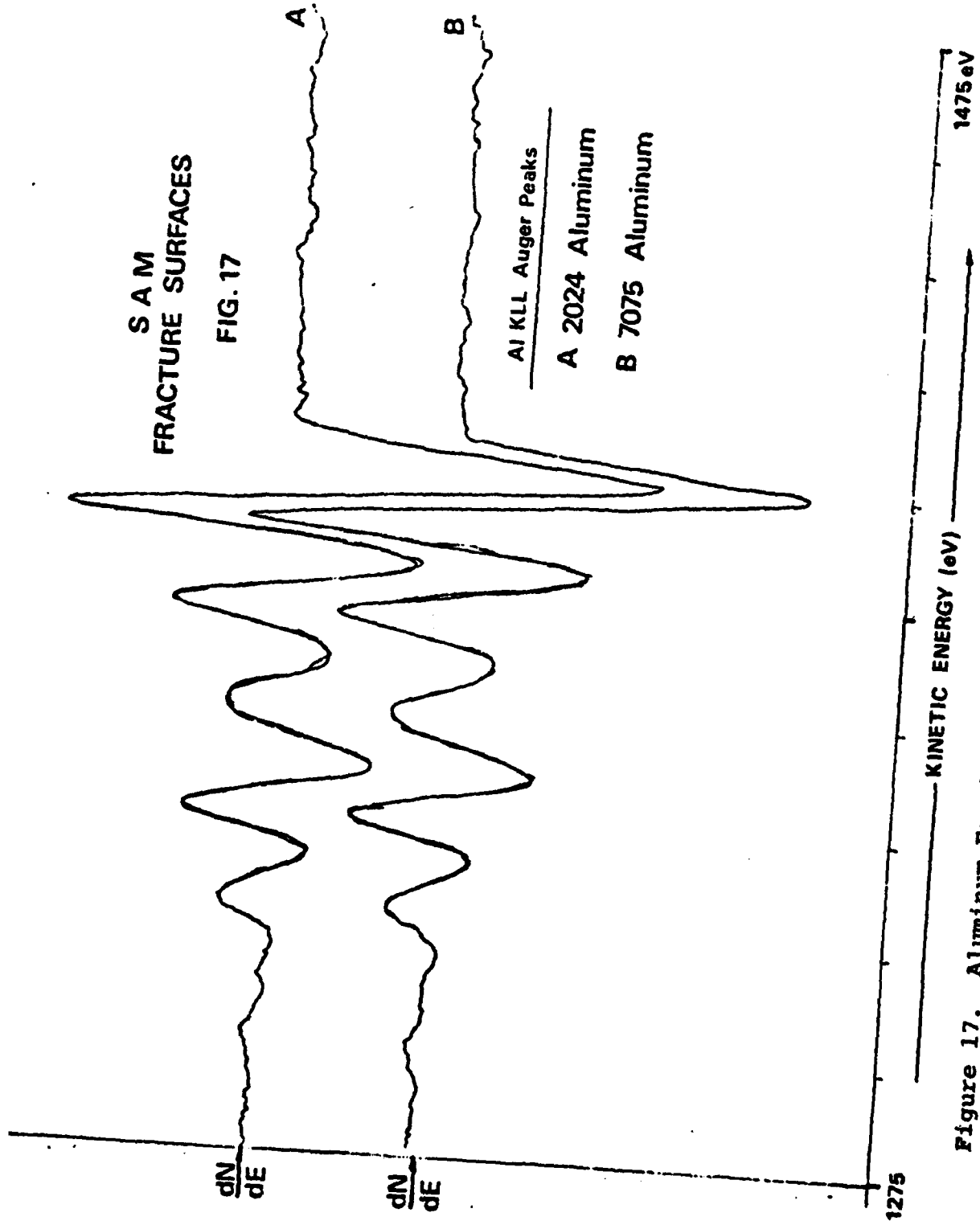
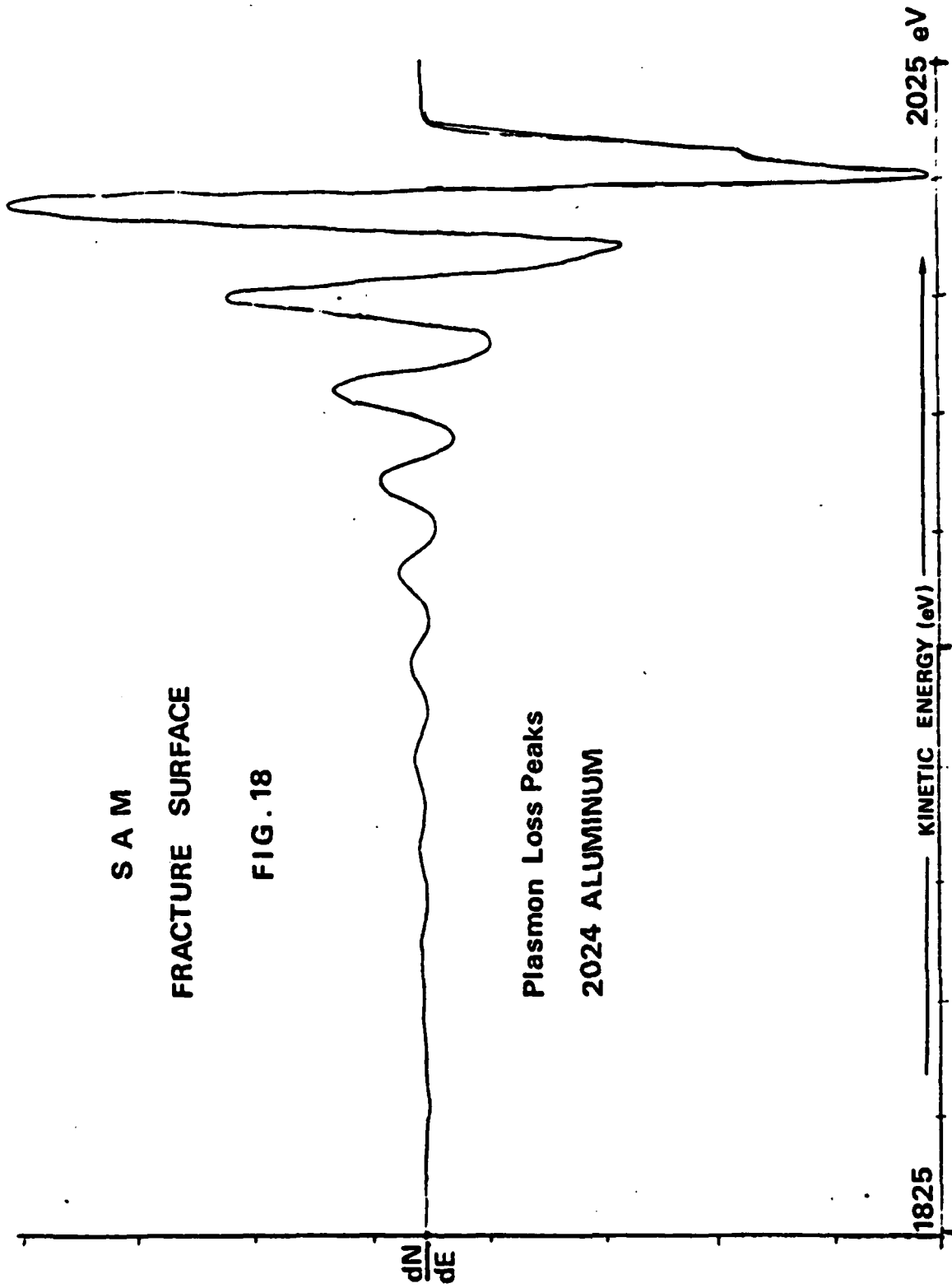


Figure 17. Aluminum Fracture Surfaces: SAM High Resolution Spectra



S A M
FRACTURE SURFACE

FIG. 18

Plasmon Loss Peaks
2024 ALUMINUM

Figure 18. 2024-T351 Aluminum Fracture Surface:
SAM High Resolution Spectrum

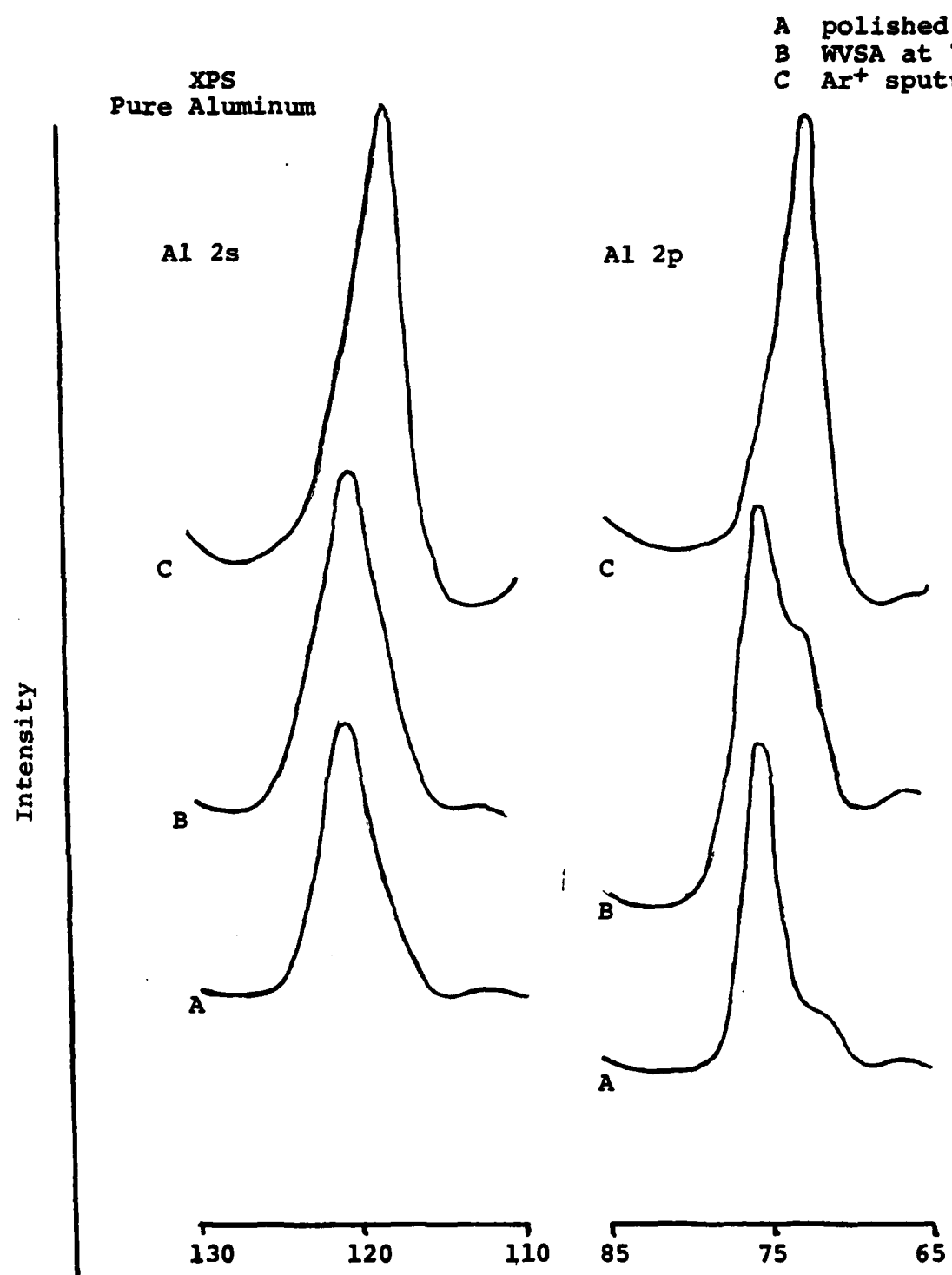


Figure 19. Pure aluminum, exposed to water vapor saturated air at 70°C for 24 hours

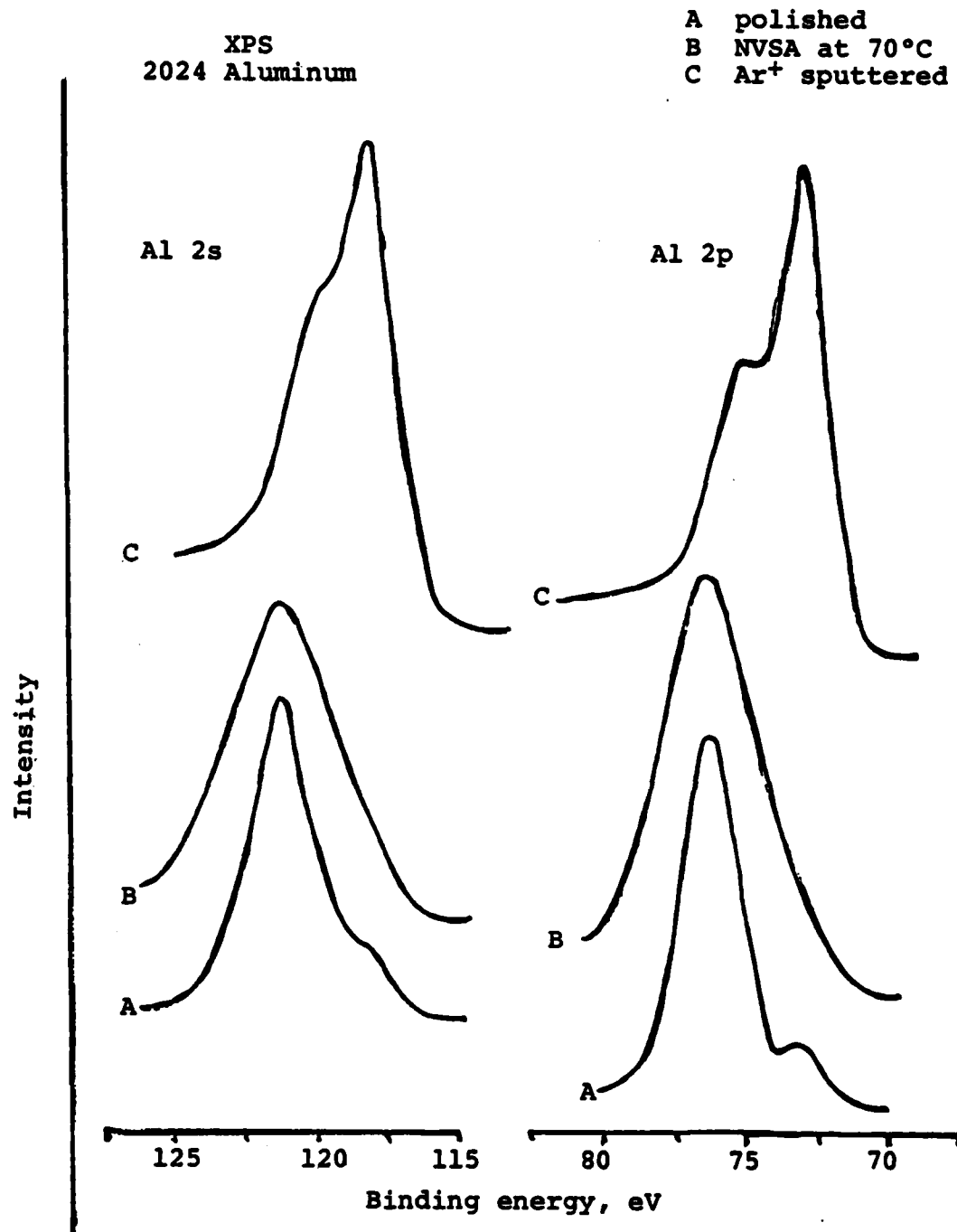


Figure 20. 2024-T351 Aluminum, exposed to water vapor saturated air at 70°C for 24 hours

A polished
B NVSA at 70°C
C Ar⁺ sputtered

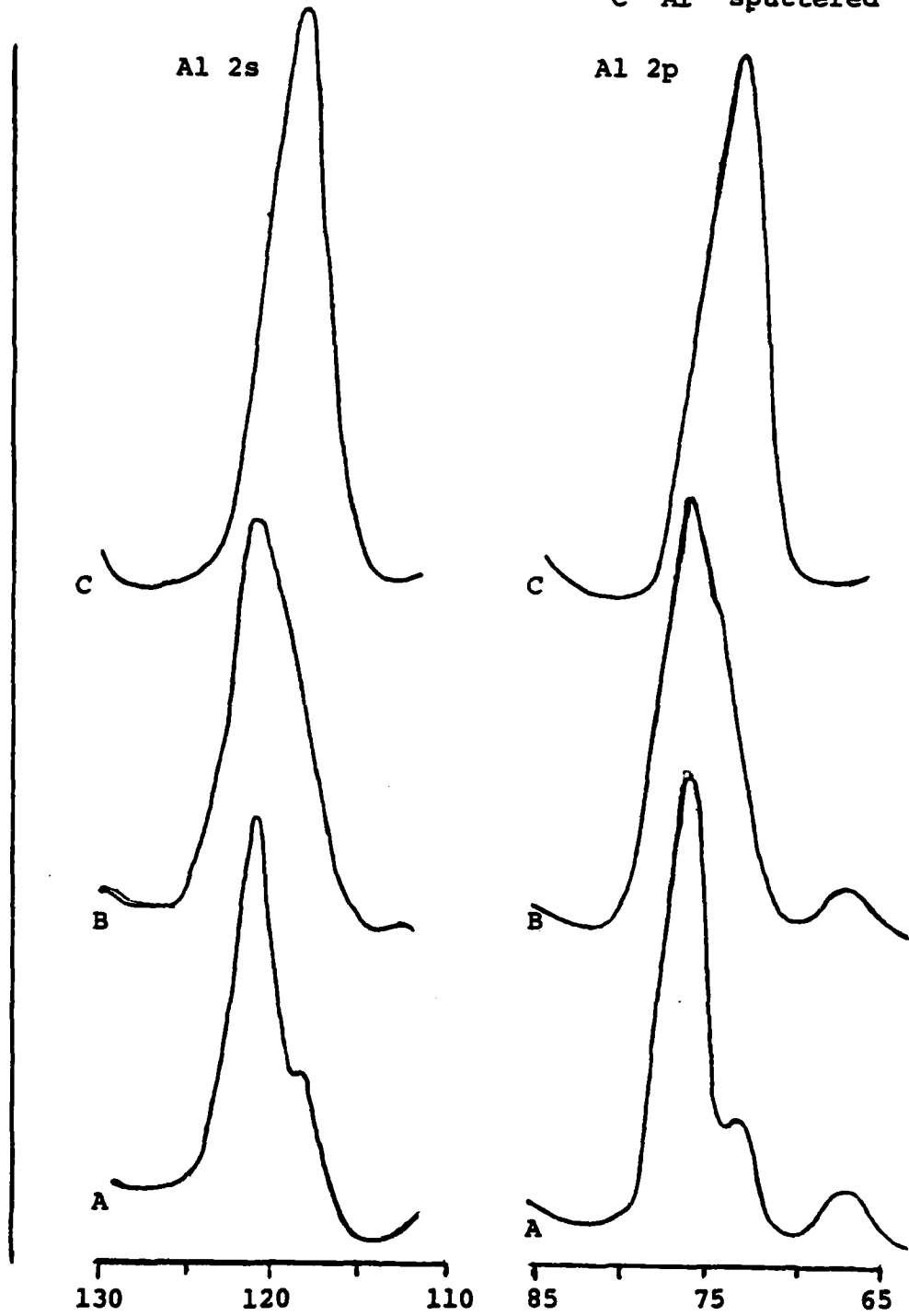


Figure 21. 7075-T351 Aluminum, exposed to water-vapor-saturated air at 70°C for 24 hours

SAM-2024 Aluminum
A Fracture
B WWSA at 70°C

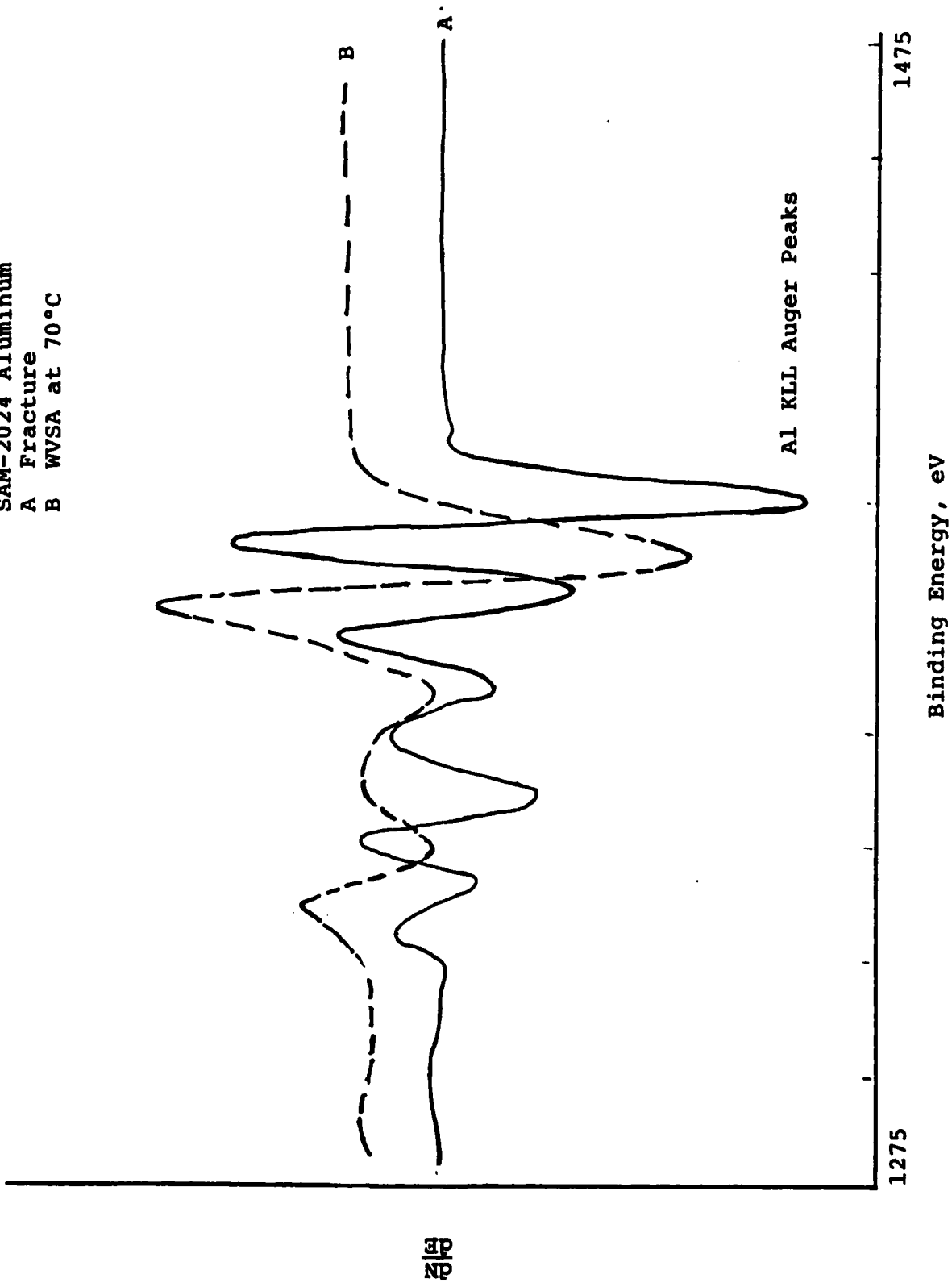


Figure 22. SAM spectra from clean Al fracture surface and from surface exposed to water-vapor-saturated air at 70°C

SAM-8075 Aluminum
A Fracture Surface
B WVSA at 70°C

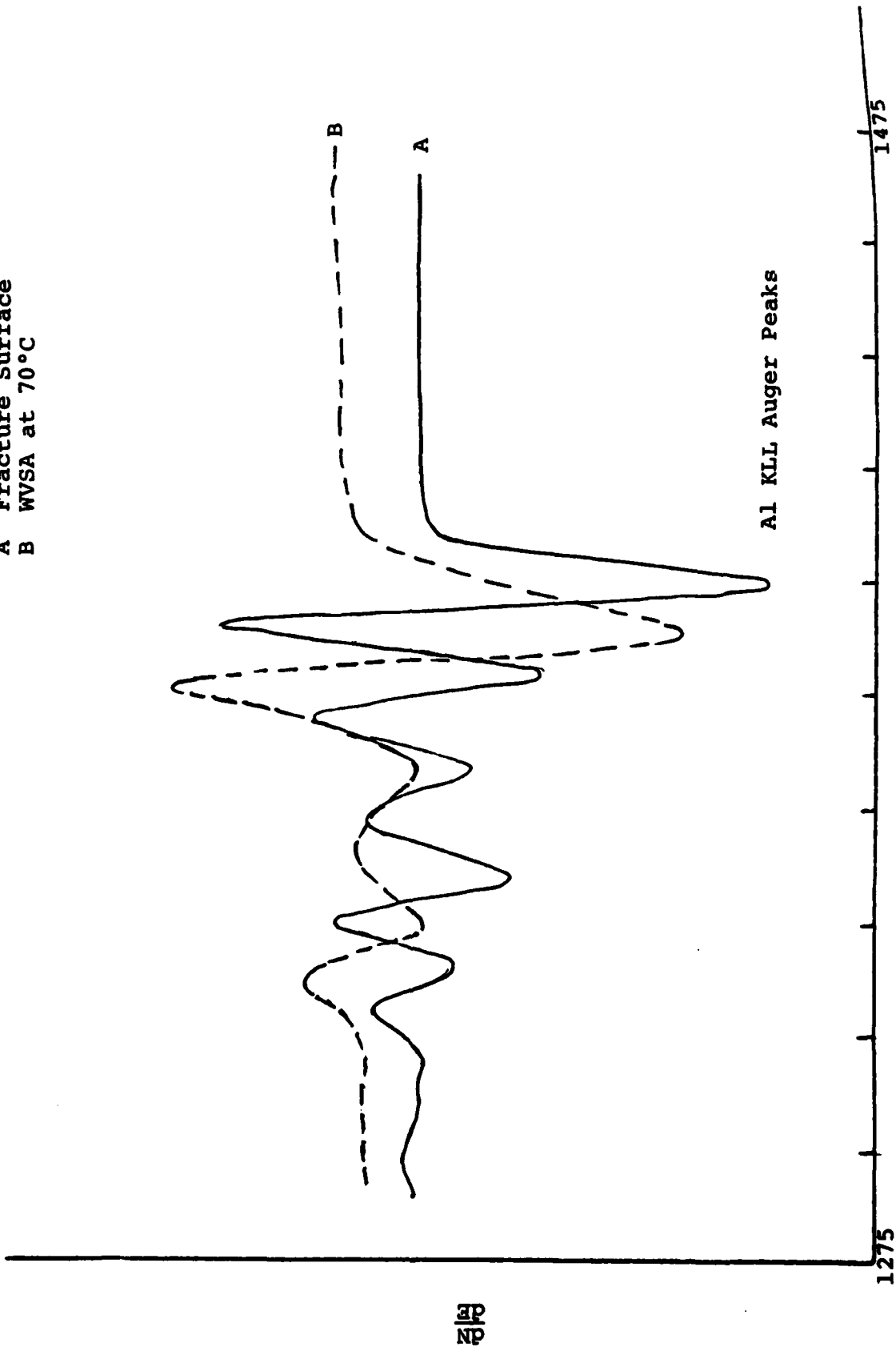


Figure 23. SAM spectra from clean Al fracture surface and from surface exposed to water-vapor-saturated air at 70°C